# Satellite-derived bathymetry for maritime archaeology: Testing its effectiveness at two ancient harbours in the Eastern Mediterranean

Kieran Westley

*School of Geography & Environmental Sciences, Ulster University, Coleraine BT52 1SA, UK*

## ARTICLE INFO

## ABSTRACT

High-resolution bathymetry is an essential tool in maritime archaeology, often used for underwater prospection, imaging, palaeo-landscape reconstruction and change detection. The commonest acquisition method relies on shipborne acoustic systems (e.g. multibeam echosounder). However, most of the world's seabed has not been surveyed using these methods. Derivation of bathymetry from high-resolution multispectral satellite imagery (Satellite-Derived Bathymetry: SDB) can redress this in shallow (<20–30 m depth) clear water. It can be derived empirically using depth control points, or independent of control data through physics-based approaches. Given global satellite coverage, it is applicable almost anywhere with suitable water conditions and is becoming increasingly widespread in the hydrographic survey community. However, archaeological application of SDB is almost totally un-investigated. This paper examines the utility of SDB for maritime archaeology through 2 case studies: the ancient harbours of Tyre (Lebanon) and Ras Ibn Hani (Syria). Tested data comprise 2 m-resolution physics-based commercial SDB and medium-resolution (10–30 m) SDB empirically derived from open access multispectral imagery (Landsat 8, Sentinel-2). SDB was assessed for its ability to detect submerged cultural features and landforms and as input into palaeo-geographic reconstructions. Tested SDB performed poorly for feature detection, but was better-suited to landform identification and palaeo-geographic reconstruction. SDB also has clear advantages: low cost, wide area coverage, speed and data availability. Disadvantages include variable accuracy, technical limitations (e.g. need for clear water) and approach-specific requirements (e.g. depth control points for empirical and complex modelling for physics-based approaches). For maritime archaeology, its current limitations means that it will not replace acoustics for prospection and imaging but it does have utility for submerged landscape investigation and reconstruction, particularly in areas which now only have no/poor bathymetric data.

## 1. Introduction

Aerial and satellite remote sensing play a key role in archaeological research and heritage management. They enable rapid cost-effective site prospection, landscape characterization, change detection and risk assessment (Cuca and Hadjimitsis, 2017; Hritz, 2014; Parcak, 2007; Philip et al., 2002; Rayne et al., 2020, 2017). Standard multispectral satellite images are highly effective for terrestrial contexts but less so for underwater environments. Water is a poor reflector of electromagnetic radiation, reflecting ~10% of received radiation versus ~50% for vegetation and ~30–40% for soils (Tempfli et al., 2009). Therefore the seabed – and by implication any submerged archaeological features - only becomes visible on multispectral imagery where the water is clear and shallow (Gao, 2009). Consequently, the role of satellite imagery in maritime archaeology has been limited to coastal, intertidal or

sometimes, very shallow-water areas (Andreou et al., 2020; Deroin et al., 2017). To image the seabed and any archaeological material lying on it, maritime archaeologists instead rely heavily on shipborne acoustic systems like sidescan sonar (SSS) or swath bathymetry generated from multibeam echosounder (MBES) or interferometric sonar. Swath systems in particular provide metre to sub-metre resolution point clouds or digital elevation models (DEMs) which are used as standard in underwater site prospection, imaging, palaeo-landscape reconstruction and change detection (Bates et al., 2011, 2013; Davis et al., 2020; Fernández-Montblanc et al., 2016; Majcher et al., 2020, 2021; Menna et al., 2018; Plets et al., 2011, 2013; Westley et al., 2011, 2019). Although MBES is now a standard seabed mapping technique and widely deployed for hydrographic, scientific and engineering purposes, the vast majority of the global seabed is unsurveyed to modern standards and covered only by low-resolution (hundreds of metres resolution) bathymetric data

(Mayer et al., 2018; Wölfl et al., 2019).

For shallow waters (<20–30 m depth), this can be redressed with Satellite-Derived Bathymetry (SDB), a technique whereby quantified seabed depths can be derived from conventional high- to medium-resolution multispectral satellite imagery (Wölfl et al., 2019). The basic technique was developed in the 1970s (Lyzenga, 1978), but computational and sensor limitations meant that its full potential has only been realized in the last decade (Heege et al., 2017; Lecours et al., 2018, 2016). The last few years have seen major developments in SDB coupled with increasing spatio-temporal coverage of accessible high-resolution satellite imagery. The end result is that viable bathymetric DEMs at metric resolution are available for shallow areas globally, either derived on a per project basis or purchased off-the-shelf from commercial providers. Consequently, SDB is increasingly used for hydrographic survey and for commercial and research applications (Collin et al., 2014; Dekker et al., 2011; Favoretto et al., 2017; Hamylton et al., 2015; Heege et al., 2017; Monteys et al., 2015; Pike et al., 2019; Poursanidis et al., 2019; Traganos et al., 2018). However, the increased accessibility of SDB does not seem to have permeated into maritime archaeology, the exception (at time of writing) being Guzinski et al. (2016). Given the known utility of bathymetric data for underwater archaeological work, at face value, SDB would seem to have great potential for maritime archaeology, particularly for coastal areas that have archaeological sites but which lack high-resolution or up-to-date bathymetry.

Therefore, this paper aims to evaluate the utility of SDB for maritime archaeology and in so doing raise awareness of the technique, highlight specific approaches and discuss limitations and/or advantages which are relevant to its archaeological use. The intention is to clarify whether it is worthwhile for maritime archaeologists to spend time or money either independently deriving SDB from freely-available satellite imagery or purchasing off-the-shelf SDB from a commercial provider. This assessment will be conducted by reference to 2 archaeological case studies from the Eastern Mediterranean: Tyre (Lebanon) and Ras Ibn Hani (Syria). Whilst not geomorphologically or sedimentologically representative of all nearshore environments in which archaeological material is found, the SDB literature indicates that the technique works in environments ranging from hard and rugged reef substrates (e.g. Hamylton et al., 2015) to level or sloping seabeds covered by sediment or vegetation (e.g. Pacheco et al., 2015; Traganos et al., 2018). Thus, the conclusions on archaeological utility which are derived from these case studies will likely also be applicable to other areas.

## 2. Background: Satellite-Derived Bathymetry

The term Satellite-Derived Bathymetry (SDB) arguably covers a range of techniques which derive water depths from space-based sensors. This includes approaches that rely on gravity measurements (Watts et al., 2020), nearshore wave characteristics (Almar et al., 2020), stereo photos (Hodúl et al., 2020), space-based laser (Parrish et al., 2019), and multispectral imagery (Salameh et al., 2019). Of these, multispectral imagery is the most widely used and associated with the concept of SDB. Thus SDB will refer solely to this approach in the rest of the paper.

It is based on the principle that amount of electromagnetic radiation (i.e. light) reflected from the seafloor is dependent on water depth. Light is attenuated by water, thus attenuation increases with depth. When viewed from above, clear shallow water appears bright because light reaches and reflects from the seafloor, whereas deep water appears dark because light is absorbed before reaching the seafloor. Other factors also play a part. Suspended sediment can also reflect or scatter light, and it can also be scattered in the atmosphere before reaching the water. The wavelength of light is also important since longer wavelengths are absorbed faster by water. Therefore, the blue (0.45–0.52 μm) and green (0.52–0.6 μm) parts of the electromagnetic spectrum tend to be used for SDB as they have the greatest through-water penetration. In theory, once water column and atmospheric effects are accounted for, the energy reflected back to a satellite should be inversely proportional to water depth (Fig. 1).

This general SDB principle is divided into two methodological categories (Gao, 2009; Salameh et al., 2019): empirical and physics-based (aka analytical, semi-analytical, radiative transfer, optimization). Empirical methods are based on obtaining the relationship between actual depths from the study area and remotely-sensed reflectance in particular spectral bands on a satellite image. This means that *in situ* depth control points are required, either derived from hydrographic charts or acquired by geophysical surveys employing acoustics, airborne LiDAR (Caballero and Stumpf, 2020; Traganos et al., 2018), or in the most recent advance, space-based laser (Ma et al., 2020). The relationship between the depth control points and remotely-sensed reflectance is then established by regression analysis. Several algorithms have been developed to model this relationship using different spectral bands or band combinations (Dierssen et al., 2003; Lyzenga, 1978; Stumpf et al., 2003). Once established, the regression coefficients can then be applied to an entire satellite image to model bathymetry at a spatial resolution equivalent to the image pixel size (Gao, 2009).

Physics-based methods rely on understanding how light is transmitted through water. The attenuation coefficients for water are not determined empirically, but are derived from modelling within a restricted range based on typical water constituents (e.g. phytoplankton, dissolved organic matter). This can be based on a Look-Up Table (LUT) of reflectance signatures representing varying combinations of depth and water constituents or purely physically-based models of reflectances with varying combinations of depth, water quality and benthic type (Dekker et al., 2011; Gao, 2009; Guzinski et al., 2016; Hamylton et al., 2015).

The advantage of both methods is that they can derive bathymetry over large areas at high spatial resolution, and at low cost compared to shipborne acoustic systems. However, both are limited to optically shallow water. In optimal conditions, maximum depths of up to 30 m have been reported, but in practice <20 m is more likely and only a few metres may be possible in turbid conditions. Both also require a clear cloud-free atmosphere and a sun-glint free water surface. Vertical uncertainties in modelled bathymetry can also be high; up to >4–5 m, though in optimal conditions they are small enough to be acceptable for safety of navigation (Dierssen and Theberge, 2016; Gao, 2009; Heege et al., 2017)

In applied terms, the main difference between empirical and physics-based methods is that the former are simpler to implement, but require depth control points from the study area. In addition, the relationship between measured depth and reflectance needs to be recalculated each time a different satellite image is used, even for the same area, and, arguably, applies only to a single substrate type (Heege et al., 2017). This hinders their applicability in areas with complex seabed substrates or rapidly changing turbid environments. That said, recent research indicates that improvements are possible through additional processing such as spatial modelling or use of multi-temporal images (Caballero and Stumpf, 2020; Cahalane et al., 2019; Da Silveira et al., 2020; Sagawa et al., 2019). Physics-based approaches do not require depth control points, but instead require input parameters relating to water and atmosphere properties which can be derived theoretically or from field measurements. In principle, they could be used in any location without prior measurement of seabed depth. However, they require knowledge of the underlying physical model or pre-prepared LUTs and the modelling required to implement them is much more complex (particularly for non-specialists) compared to the empirical approaches (Gao, 2009; Guzinski et al., 2016).

## 3. Study areas

Application of SDB is shown by reference to Tyre (Lebanon) and Ras Ibn Hani (Syria) (Fig. 2). From the standpoint of technical requirements, these areas have reasonably clear water, extensive cloud-free satellite image coverage and, for empirical SDB, control depths from
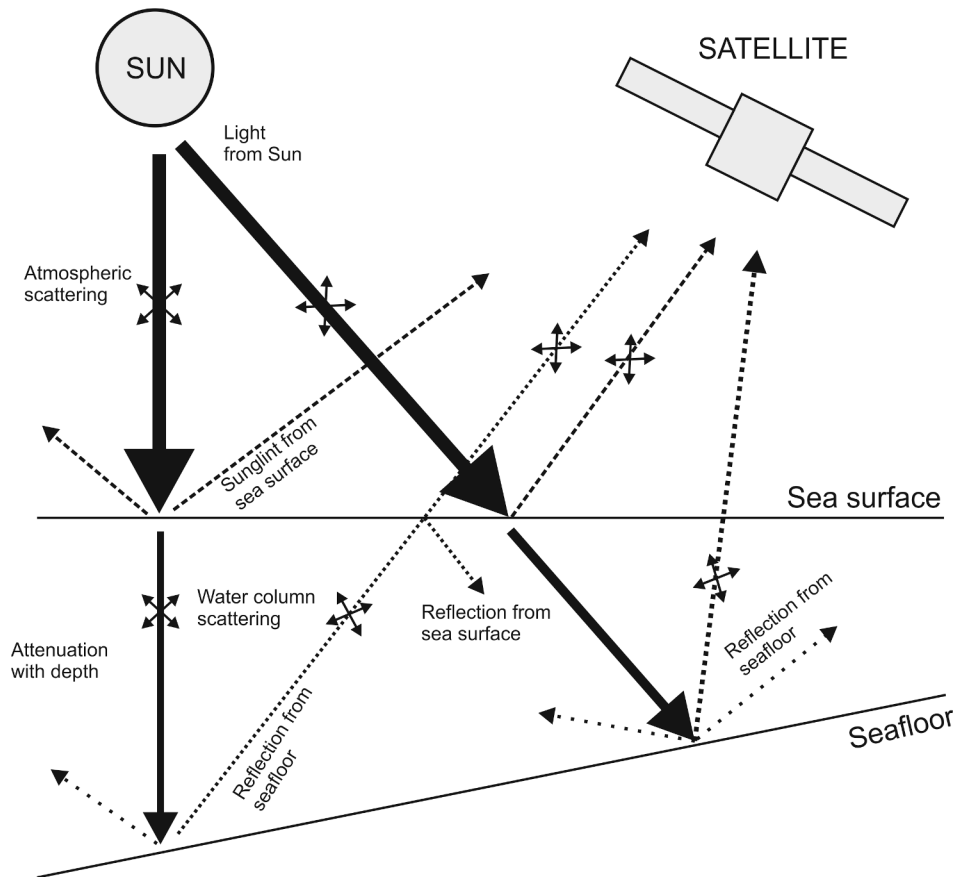
**Fig. 1.** Schematic representation of SDB. Multiple scatterers in the atmosphere and water decrease the signal returning to the satellite. Not shown are seafloor variations (e.g. substrate) which also affect the returning signal via differential absorption or scattering.

hydrographic charts. These sites are also archaeologically significant ancient harbours and thus representative of the types of coastal or shallow water archaeological sites to which SBD might conceivably be applied.

Tyre was occupied from the Bronze Age onwards and probably contained a series of ancient harbour complexes, including on the mainland and the northern and southern sides of the peninsula. It was a major seaport throughout the Phoenician, Hellenistic, Roman and Byzantine periods with its importance declining thereafter (Marriner et al., 2008, 2005). The majority of these harbour complexes are now buried under coastal sediment, but submerged remains are also present. These include a Phoenician jetty off the modern harbour and a drowned urban quarter containing structural remains, polder walls and quarries on the southwestern side of the peninsula (Marriner et al., 2008; Noureddine, 2010; Noureddine and Mior, 2013; Semaan, 2016).

Ras Ibn Hani was occupied from the Late Bronze Age onwards and formed part of the kingdom of Ugarit, possibly functioning as a suburban quarter to the nearby Ugaritic capital at Ras Shamra. It has been suggested that it provided sheltered anchorages and landing places on both the northern and southern sides of the modern peninsula. Ancient harbour infrastructure (partly submerged moles and jetties) is present on either side of this peninsula. These structures lack absolute dates, although Bronze/Iron Age to Hellenistic ages have been suggested. Following the collapse of Ugarit (c. 1190 BCE), archaeological evidence suggests Ras Ibn Hani remained occupied during the succeeding Iron Age, Persian and Hellenistic periods (Carayon, 2008; Marriner et al., 2012)

## 4. Methodology

Two SDB products were used. Firstly, fully-processed high-resolution SDB from a commercial provider (EOMAP). These data cover ~23 km² around Tyre and ~28 km² around Ras Ibn Hani. They were derived from Worldview-2 (Ras Ibn Hani) or Pleiades (Tyre) imagery using proprietary physics-based algorithms and were supplied at 2 m spatial resolution with vertical and horizontal accuracies of 1 m +/- 15% water depth and 5 m respectively.

Secondly, SDB empirically derived from freely-available medium-resolution satellite imagery (Landsat 8, Sentinel-2: Table 1). Images were chosen to minimize cloud cover, sun-glint, surface waves and sediment plumes. Two empirical algorithms were tested for each study area. Firstly, the linear band ratio of Lyzenga (1978):

$$Z = a_0 + a_i X_i + a_j X_j \tag{1}$$

where $Z$ = estimated depth, $a_0$, $a_i$ and $a_j$ = tuneable constants determined by multiple linear regression of $X_i$ and $X_j$ against control depths. The value of $X$ is determined from:

$$X_i = \ln[R_w(\lambda_i) - R_\infty(\lambda_i)] \tag{2}$$

where $R_w(\lambda_i)$ = reflectance from image band $i$ and $R_\infty(\lambda_i)$ = the average reflectance from deep water from band $i$. Bands $i$ and $j$ are usually the blue and green bands.

Secondly, the ratio-transformation of Stumpf et al. (2003):

$$Z = m_1 \frac{\ln(n R_w(\lambda_i))}{\ln(n R_w(\lambda_j))} - m_0 \tag{3}$$

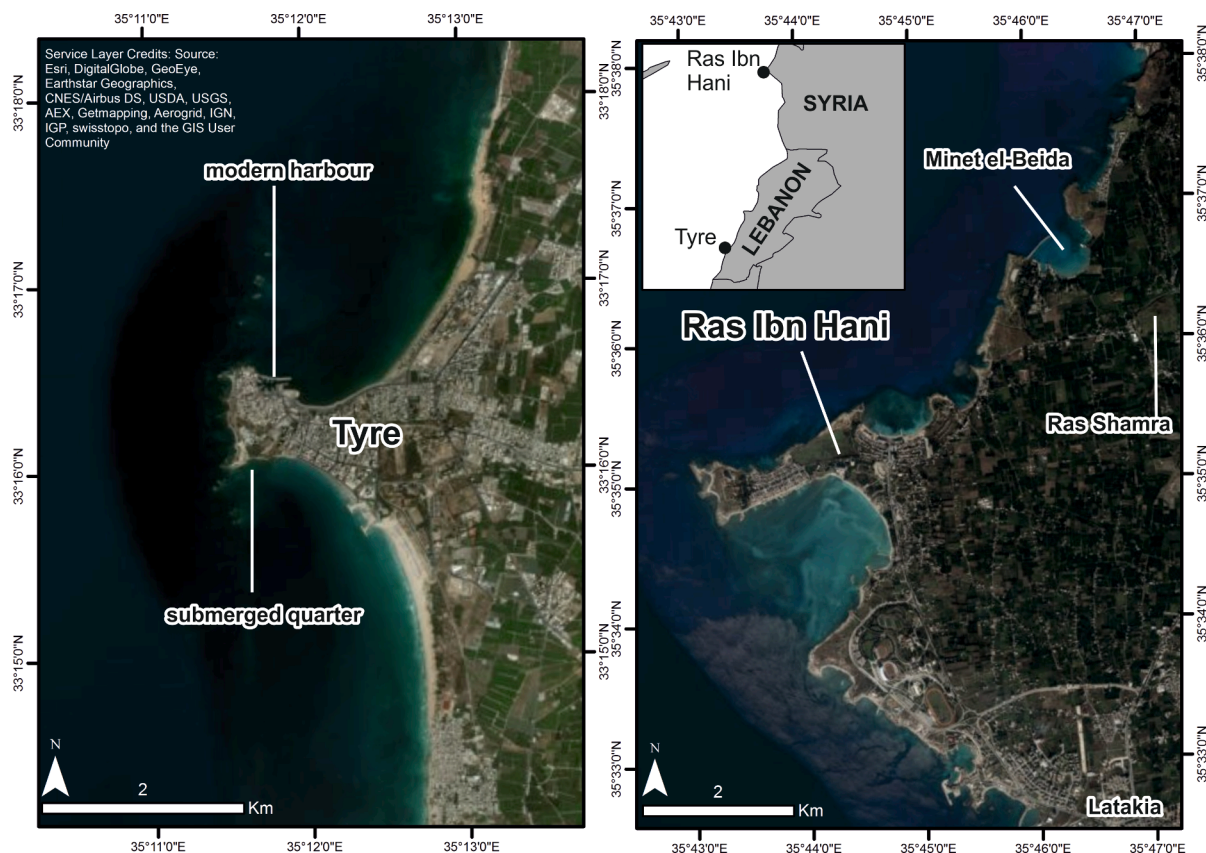where $Z$ = estimated depth, $n$ = fixed constant to ensure positive log

**Fig. 2.** Satellite images showing Tyre (left) and Ras Ibn Hani (right). Both locations are modern peninsulas which were formerly offshore islands that were subsequently joined to the mainland by tombolos (Marriner et al., 2012, 2005). Inset map shows general location in the Eastern Mediterranean.

**Table 1**
Satellite images used in the empirical SDB tests.

| Site | Satellite | Pre-processing level | Acquisition date | Path/row | Spatial Resolution | Source |
|------|-----------|---------------------|------------------|----------|-------------------|--------|
| Tyre | Landsat 8 | Collection 1 Level 1 | 13/04/2018 | 174/037 | 30 m | USGS Earth Explorer |
| Tyre | Sentinel-2A | Level 1C | 18/09/2017 | T36SXB | 10 m | Copernicus Open Access Hub |
| Ras Ibn Hani | Landsat 8 | Collection 1 Level 1 | 05/02/2017 | 174/035 | 30 m | USGS Earth Explorer |
| Ras Ibn Hani | Sentinel-2A | Level 1C | 02/11/2018 | T36SYB | 10 m | Copernicus Open Access Hub |

values, $R_w$ = reflectance from image bands $i$ and $j$ (respectively usually the blue and green bands), $m_1$ and $m_0$ = respectively tuneable constant and offset used to scale and adjust the ratio to depth. $m_1$ and $m_0$ are found by linear regression of the log-transformed band ratios against control depths. A modified version of Equation (3) which omits $n$ was used here following (IHO, 2016) and (Traganos et al., 2018).

These basic algorithms are the most widely used in SDB and underpin many recent and more complex SDB approaches (Caballero and Stumpf, 2020; Cahalane et al., 2019; Casal et al., 2019; Pacheco et al., 2015). Both algorithms were applied following IHO (2016). This requires only standard GIS software (ArcGIS 10.3 in this case) and is suitable for non-specialists. The full workflow is in IHO (2016), therefore only additional study-specific inputs or variations are shown below. These included:

1. Image pre-processing: atmospheric correction (Dark Spectrum Fitting: Vanhellemont and Ruddick, 2018) and sun-glint correction were performed in open source ACOLITE (v. 20180925.0) software (Vanhellemont, 2018).

2. Control depths: manually digitized from georeferenced hydrographic charts. Tyre is covered by Admiralty Chart 1561-4 which combines soundings from surveys dated to 2010–11 and 1920–21. In total, 244 soundings ranging from −0.2 m to −34 m were digitized. Ras Ibn Hani is covered by Admiralty Chart 1579-3. Updates to this chart are

lacking; soundings are based on a survey from 1861. In total, 73 soundings (range of −2.1 m to −44 m) were digitized. Although it might be preferable to have control depths from recent geophysical surveys (as used in many empirical SDB research studies), the use of hydrographic charts allows a more realistic assessment of areas which lack such recent surveys (see also Caballero and Stumpf, 2020).

3. Algorithm variants (Table 2): Lyzenga (1978) is generally implemented using the blue and green bands of a satellite image. In addition,

**Table 2**
Summary of SDB algorithm variants used in this study.

| Variant | SDB algorithm | Bands used | Regression relationship |
|---------|--------------|------------|------------------------|
| Lyzenga B1-2-3 | Lyzenga (1978) | Coastal aerosol, blue, green | Multiple linear |
| Lyzenga B2-3 | Lyzenga (1978) | Blue, green | Multiple linear |
| Lyzenga B3-4 | Lyzenga (1978) | Green, red | Multiple linear |
| Stumpf Linear | Stumpf et al. (2003) | Blue, green | Linear |
| Stumpf Exponential | Stumpf et al. (2003) | Blue, green | Exponential |
| Stumpf Polynomial | Stumpf et al. (2003) | Blue, green | 2nd order polynomial |

this study also tested a coastal aerosol-blue-green combination (following Pacheco et al. 2015) and a green–red combination (following Gao, 2009 which suggests a shift to long wavelengths with increased turbidity). All implementations of Stumpf et al. (2003) used only the blue and green bands. Variants instead focused on the regression relationship between band ratios and control depths. Three relationship variants were tested: linear (following IHO, 2016), 2nd order polynomial (Dierssen et al., 2003) and exponential (Traganos et al., 2018).

The performance of the empirically-derived bathymetry was assessed by comparing between different algorithms and variants, and by comparison with the commercial SDB. Qualitatively exploring the effectiveness of both data types for maritime archaeology was done by reference to a) feature detection and b) palaeo-landscape mapping. These are key archaeological topics to which high-resolution bathymetric data can contribute (Plets et al., 2011; Westley et al., 2011). Feature detection assessed whether the SDB could resolve submerged features of archaeological interest and is therefore useful for prospection or record enhancement. Palaeo-landscape mapping tested the effectiveness of the SDB as an input into palaeo-geographic reconstruction and for detecting submerged landforms which could be remnants of former terrestrial landscapes. Feature detection requires high spatial resolution data compared to palaeo-landscape mapping (Plets et al., 2013), therefore only the commercial SDB was used for this. Conversely, palaeo-landscape mapping used both empirical and commercial datasets.

## 5. SDB results

### 5.1. Commercial SDB overview

The commercial SDB shows that the mainland coast of the Tyre peninsula is fronted by a slope which leads to a deeper (−8 m to −12 m) flat-bottomed channel (Fig. 3A). Away from the peninsula, the slope transitions to a 500–600 m-wide platform which reaches depths of −3 m to −4 m before dropping sharply to the channel. The seaward side of the channel comprises a 1–4 m high submerged ridge which links to the shallow exposed reef on Tyre's outer coast. South of the peninsula, the submerged ridge divides, and possibly extends to the southernmost extent of data coverage. Extension of the ridge beyond ~2.4 km north from the peninsula is not evident. The SDB also resolves a 300 m-long linear channel located 3.7 km north of the peninsula. This is a dredged channel probably related to the construction of a breakwater/pier, visible on satellite imagery from 2016 onwards.

For Ras Ibn Hani, the SDB shows that the large bay south of the peninsula comprises a gently sloping platform with depths of −2 m to −4 m (Fig. 3B). The platform is terminated by a steep slope to depths of −12 m to −14 m. The same general morphology characterizes the bays north of the peninsula (Minet el-Ouabban and Minet el-Helu). Minet el-Beida further to the north differs since it is has a regular slope rather than a platform. The rest of the coast is characterized by platforms of varying width (metres to low hundreds of meters) which are terminated
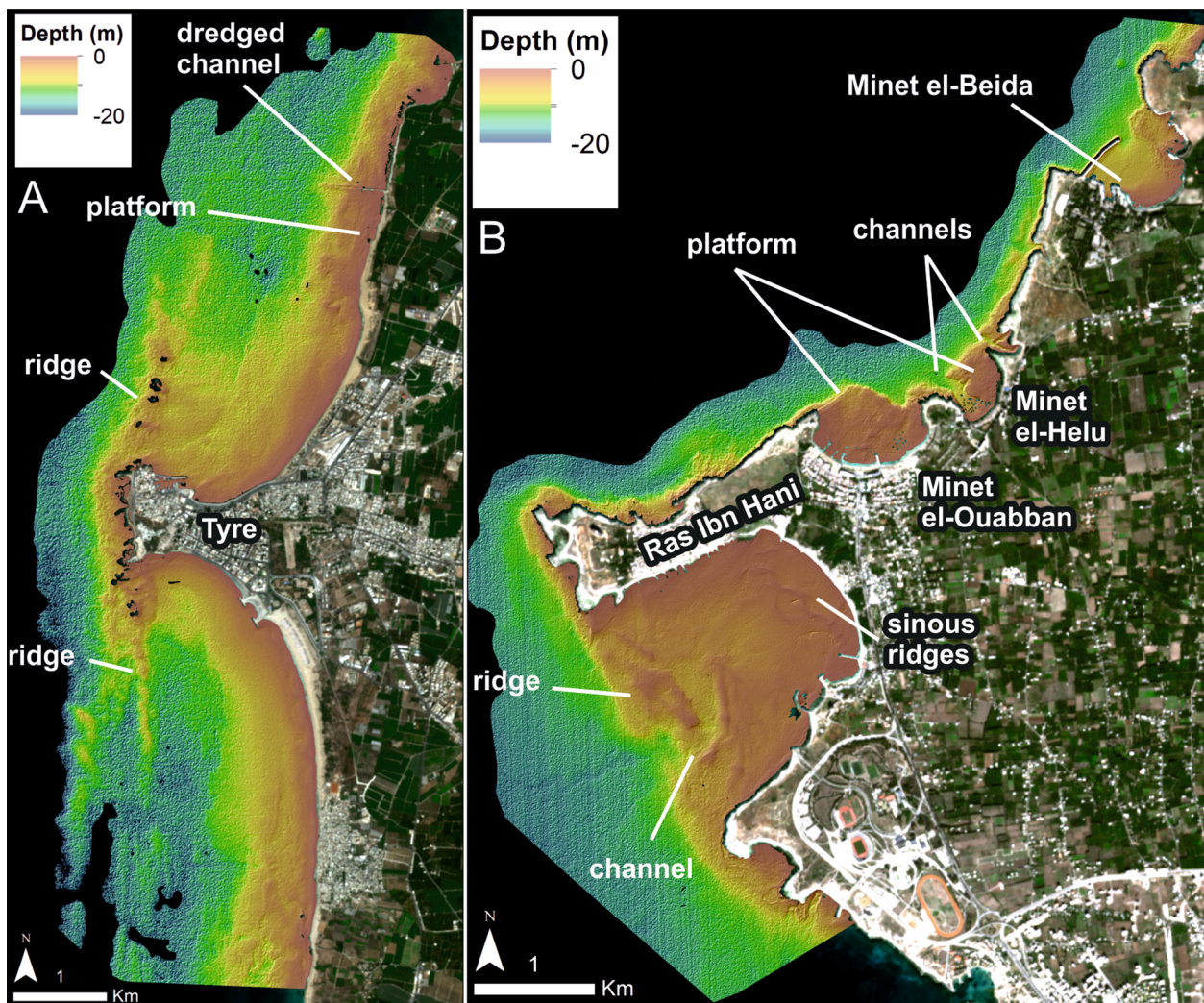


**Fig. 3.** Hillshaded 2 m-resolution commercial SDB for a) Tyre and b) Ras Ibn Hani.

by steep slopes or edges. Other submerged landforms are also evident. The southern bay has a north–south orientated channel (max depth −7 m) which is flanked by upstanding ridges, and a series of sinuous northwest-southeast running ridges, up to 1 m high. Channels cut into the platform are also visible at Minet el-Helu.

### 5.2. Empirical SDB results

#### 5.2.1. Tyre

All empirical SDB variants resolved the general bathymetry observed in the high-resolution commercial SDB, specifically the shallow inshore platform, platform slope/edge, deeper channel and submerged ridges (Supplementary Figs. S1 and S2). It is also evident that most variants can resolve breaks in the ridge and its branching south of the peninsula. Other identifiable features include a large submerged inlet ~ 7.5 km north of the peninsula. However, there are also differences between

algorithms and/or variants.

Firstly, noise is present, most clearly seaward of the submerged ridge (e.g. Figs. S1a, d, e, f; Fig. S2a, d, e, f). This manifests as diffuse areas of apparently shallow bathymetry and is probably false bathymetry created by suspended sediment, or surface effects (waves, glint) which were not fully eliminated by pre-processing. Secondly, there are difference in absolute depth values. For example, the Stumpf linear (Figs. S1b and S2a) and all Lyzenga variants (Fig. S1c, d, e; Fig. S2c, d, e) show bathymetry seaward of the submerged ridge whereas the Stumpf polynomial and exponential variants suggest that the same areas are beyond the maximum resolvable depth.

These differences are further highlighted by comparing two shore-normal transect profiles located north and south of the Tyre peninsula (Fig. 4). For Transect 1, the Sentinel-2 SDB show generally good agreement with the exception of deeper water seaward of the ridges and the shallow inner platform. Here vertical differences of up to 4 m are
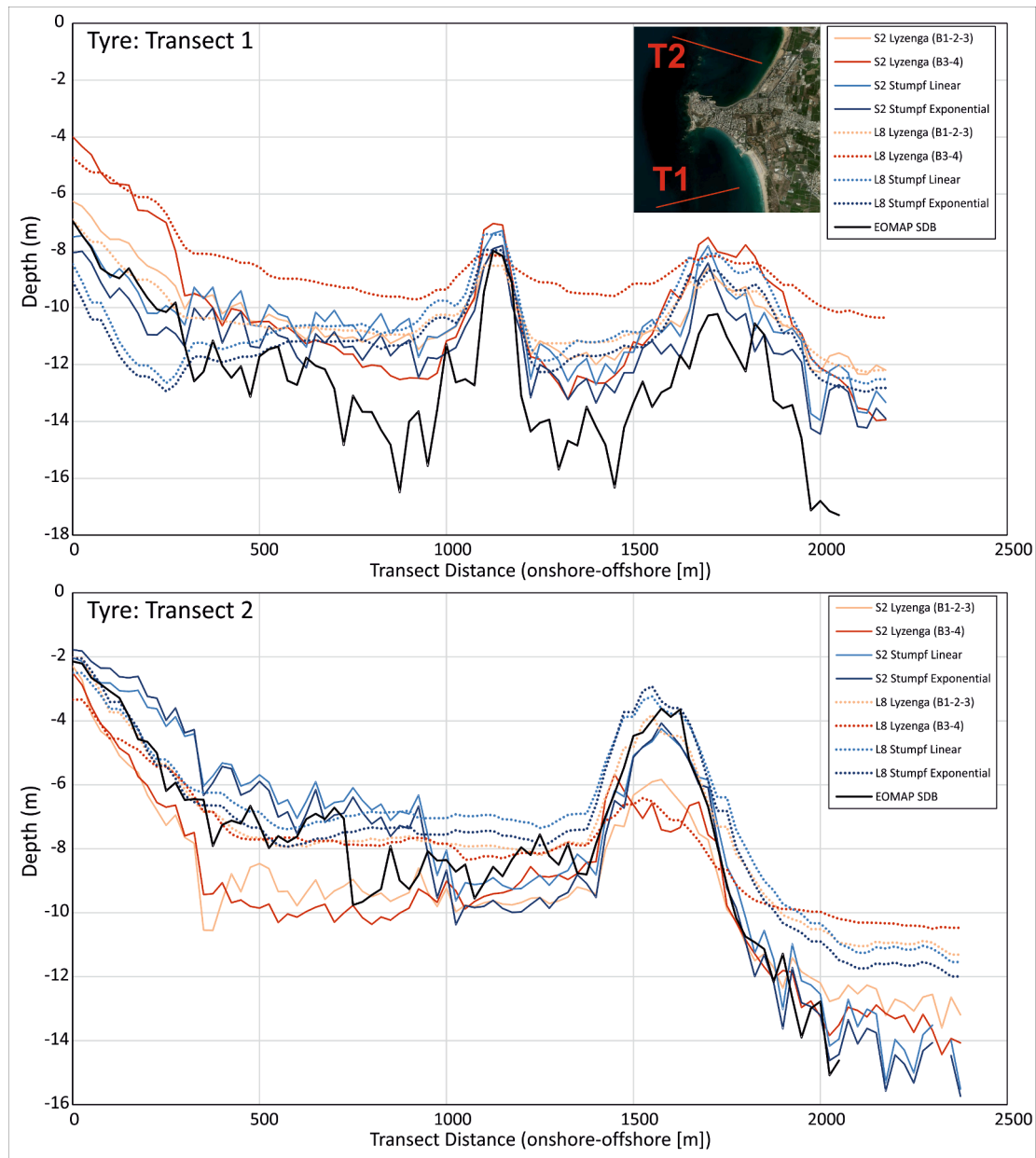


**Fig. 4.** Bathymetric profiles from Tyre (see inset image for location) showing SDB algorithm variants applied to both Landsat 8 (dotted line) and Sentinel-2 data (solid line). Lyzenga B2-3 and Stumpf Polynomial variants omitted for clarity since they are very similar to Lyzenga B1-2-3 and Stumpf Exponential respectively. Black line is the equivalent commercial SDB transect.

evident and with Lyzenga B3-4 considerably under-predicting compared to the other Sentinel-2 variants. The Landsat 8 SDB data show an even larger range; up to 6 m for the inner platform between the Stumpf Exponential and Lyzenga B3-4 variants. It is also evident that the Landsat 8 Lyzenga B3-4 and all Stumpf variants predict a more subdued ridge-channel topography compared to the other variants. For Transect 2, the Landsat 8 data show closer correspondence with <2 m vertical difference. The same is true for the Sentinel-2 SDB except for the inner part of the platform (400–1000 m distance) where up to 4 m vertical difference is apparent. The Transect 2 profiles also suggest that Landsat 8 tends to under-predict compared to Sentinel-2.

### 5.2.2. Ras Ibn Hani

All empirical SBD variants resolved the general bathymetry around Ras Ibn Hani, including the shallow water platform, steep edge/drop-off, and the narrow channel at the mouth of the southern bay. However, there are also differences between algorithms and/or variants (Figs. S3 and S4).

Some variants are clearly affected by false bathymetry which is manifest by apparently shallow areas seaward of the coastal platforms. Absolute depths also vary between different variants. For example, the Stumpf Linear and Lyzenga variants are not able to derive accurate depths in very shallow water (e.g. Fig. S3a; f; Fig. S4a; d; e). In these
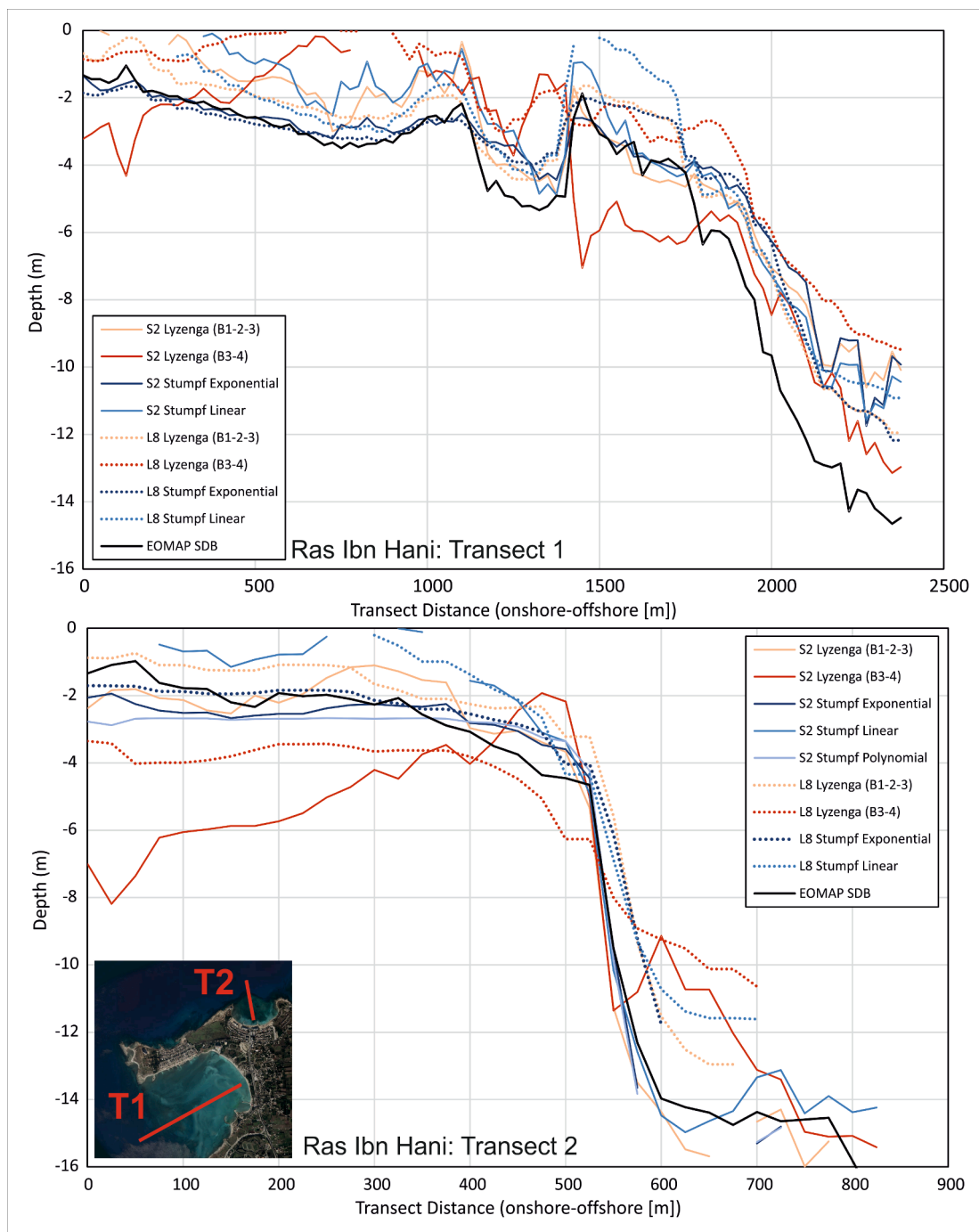


**Fig. 5.** Bathymetric profiles from Ras Ibn Hani (see inset image for location) showing SDB algorithm variants applied to both Landsat 8 (dotted line) and Sentinel-2 data (solid line). Note that Lyzenga B2-3 and Stumpf Polynomial variants omitted for clarity as they are very similar to Lyzenga B1-2-3 and Stumpf Exponential respectively. Black line is the equivalent commercial SDB transect.

cases, gaps are present in the bay south of Ras Ibn Hani because derived depths were above sea-level, and hence excluded.

These differences are further highlighted by transect profiles located north and south of the Ras Ibn Hani peninsula which cross the shallow inner platform and drop-off to deeper water (Fig. 5). Transect 1 has reasonable correspondence between some variants, mainly Lyzenga B1-2–3, Stumpf Exponential and Stumpf Linear. These show well the drop-off, shallow platform and the channel and ridge at the bay mouth. Even so, vertical differences of up to 1–2 m, for instance over the ridge, are evident. Larger vertical differences (up to 4 m) are apparent when compared to Lyzenga B3-4, which appears to show opposed patterns over the shallow platform, ridge and channel for both Sentinel-2 and Landsat 8. For Transect 2, the basic pattern is the same (platform, drop-off, deeper seabed), with good correspondence over the drop-off and greater differences over the platform and deeper seabed. Again, Lyzenga B3-4 appears to be the outlier for both Sentinel-2 and Landsat 8, particularly over the shallow platform where differences of 4–6 m are apparent. For the remaining variants, vertical differences over the platform range from 1 to 3 m.

*5.3. Empirical and commercial SDB Comparison*

One clear difference between the empirical and commercial SDB is the maximum resolvable depth. The latter reached depths of almost −20 m, where the former reached depths of −12 m (Landsat 8) and −15 m (Sentinel 2). To enable further quantifiable comparison, 100 randomly placed sample depths were extracted from each empirical SDB variant and plotted against equivalent samples from the commercial SDB (Figs. S5, S6; Table 3). This highlights that the empirical approaches tend to under-predict bathymetry for depths > c. −4 to −6 m. This under-prediction is accentuated to varying degrees depending on the empirical variant is used. It is also clear that general correspondence with the commercial SBD varies with area and algorithm variant. Thus, Ras Ibn Hani has the variant with the overall lowest but also highest RMSE (Landsat 8 Stumpf Expo and Lyzenga B3-4 respectively). It also shows a tendency for lower RMSE for Landsat 8 and Lyzenga variants (<2 m). Conversely, Tyre has in general higher, but more consistent RMSE values than Ras Ibn Hani. The lowest RMSE for this area are also achieved with Lyzenga variants, but, in contrast to Ras Ibn Hani, with Sentinel 2 data. These differences could relate partly the variable nature of the control depths used: Tyre had more points including from a recent survey, and thus might be expected to provide a more consistent training dataset resulting in less variation in the derived bathymetry.

The variable correspondence between the commercial and empirical SDB is further highlighted by comparing the transect profiles. Other than localized discrepancies, the main difference apparent from these is the tendency for empirical variants to under predict bathymetry in deeper water. This could result from a shoal bias in the control depths or sub-optimal image (e.g. turbidity offshore). In terms of individual algorithms, Lyzenga B1-2-3 and B2-3 are very similar as are Stumpf Polynomial and Exponential. The largest differences seem to occur with Lyzenga B3-4 which consistently gave the most different profiles. In terms of satellite sensor, no clear pattern was observed when comparing Landsat 8 and Sentinel 2.

Notwithstanding these vertical discrepancies, it is also apparent that the best performing empirical SDB variants are capable of resolving general seabed morphology, with ridges, deeps and slopes in the correct spatial location (Figs. 4 and 5). Based on the RMSE and error range, these are Lyzenga B2-3 and Stumpf Polynomial for Tyre and Lyzenga B1-2–3 and Stumpf Exponential for Ras Ibn Hani. Thus the next step is to apply the SDB to archaeological questions of feature detection and palaeo-landscape mapping.

**Table 3**

R² values (indicative of how well the SDB algorithm variants fit their trendlines), Root Mean Square Error (RMSE: average difference with the reference EOMAP dataset) and error range (full range of difference with the reference EOMAP dataset).

| Area | Satellite | SDB algorithm | R² | RMSE (m) | Range (m) |
|---|---|---|---|---|---|
| Ras Ibn Hani | Landsat8 | Lyzenga B1-2-3 | 0.97 | 1.72 | 5.3 |
| Ras Ibn Hani | Sentinel2 | Lyzenga B1-2-3 | 0.87 | 2.21 | 9.3 |
| Ras Ibn Hani | Landsat8 | Lyzenga B2-3 | 0.97 | 1.74 | 5.1 |
| Ras Ibn Hani | Sentinel2 | Lyzenga B2-3 | 0.88 | 2.14 | 7.7 |
| Ras Ibn Hani | Landsat8 | Lyzenga B3-4 | 0.77 | 4.02 | 14.6 |
| Ras Ibn Hani | Sentinel2 | Lyzenga B3-4 | 0.59 | 3.68 | 20.9 |
| Ras Ibn Hani | Landsat8 | Stump Polynomial | 0.81 | 2.32 | 13.7 |
| Ras Ibn Hani | Sentinel2 | Stump Polynomial | 0.85 | 2.26 | 9.3 |
| Ras Ibn Hani | Landsat8 | Stumpf Exponential | 0.96 | 1.57 | 5.6 |
| Ras Ibn Hani | Sentinel2 | Stumpf Exponential | 0.88 | 2.21 | 9.1 |
| Ras Ibn Hani | Landsat8 | Stumpf Linear | 0.92 | 2.75 | 7 |
| Ras Ibn Hani | Sentinel2 | Stumpf Linear | 0.86 | 2.29 | 7.7 |
| Tyre | Sentinel2 | Lyzenga B1-2-3 | 0.83 | 2.52 | 11.3 |
| Tyre | Landsat8 | Lyzenga B1-2-3 | 0.84 | 2.86 | 10 |
| Tyre | Sentinel2 | Lyzenga B2-3 | 0.83 | 2.46 | 9.8 |
| Tyre | Landsat8 | Lyzenga B2-3 | 0.78 | 3.18 | 11.3 |
| Tyre | Sentinel2 | Lyzenga B3-4 | 0.8 | 2.46 | 11.1 |
| Tyre | Landsat8 | Lyzenga B3-4 | 0.8 | 3.56 | 12.4 |
| Tyre | Sentinel2 | Stump Polynomial | 0.77 | 2.56 | 11.4 |
| Tyre | Landsat8 | Stump Polynomial | 0.79 | 2.78 | 11.8 |
| Tyre | Sentinel2 | Stumpf Exponential | 0.77 | 2.83 | 10.4 |
| Tyre | Landsat8 | Stumpf Exponential | 0.79 | 3.05 | 11.8 |
| Tyre | Sentinel2 | Stumpf Linear | 0.75 | 2.83 | 10.9 |
| Tyre | Landsat8 | Stumpf Linear | 0.74 | 3.45 | 13 |

## 6. Feature detection

### 6.1. Tyre

Although Tyre has functioned as a harbour since the Bronze Age, the closest (published) ancient wreck is a 4-6th Century BCE cargo scatter to its northwest and at −34 m depth; i.e. beyond the SDB range (Seco Alvarez, 2012: cited in Semaan, 2016). Charted wrecks include a cluster of obstructions and one modern wreck (MV *Eko*, lost 1976) immediately north of the harbour and another wreck (unknown name) 930 m northwest of the harbour in −9.7 m depth. The commercial SDB do not show upstanding anomalies at the charted locations. However the nature of the obstructions and the unknown wreck (e.g. size, height) are not described in hydrographic reportage (Wrecksite.eu, 2020). Therefore it is unclear if they are theoretically resolvable by the SDB. For the MV *Eko,* there are no post-1990 descriptions of the wreck (Wrecksite.eu, 2020). Earlier reports indicated that she lay with her bow and stern section showing and blocking the harbour entrance. Very high-resolution (VHR: <1 m) Google Earth images show one instance of a possible feature at this location (Fig. 6). It is therefore possible that the wreckage is low-lying and not resolvable because it lies within the vertical uncertainty of the SDB. Also, the lack of a clear signature on even VHR satellite imagery means that it is unlikely that this wreck would be detectable by 2 m-resolution SDB (Fig. 6).

Underwater archaeological investigations on the northern side of the harbour have identified an 85–95 m-long Phoenician jetty running
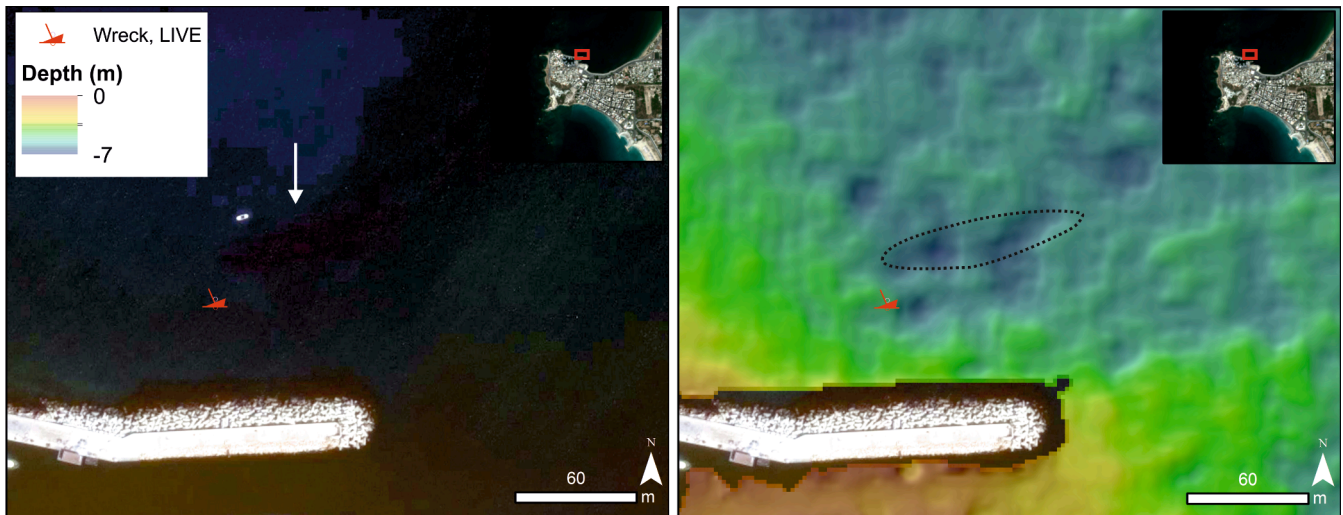
**Fig. 6.** Comparison of VHR satellite image (left: Google Earth, 24/9/2014) and commercial SDB (right) off Tyre's north harbour (see inset image for location). The faint oval-shaped anomaly (indicated by arrow) on the VHR image corresponds roughly to the charted position of MV Eko (red symbol), but lacks surface expression on the SDB (dashed oval shows anomaly position). (For interpretation of the references to colour in this figure legend, the reader is referred to the web version of this article.)

parallel to the modern breakwater at a depth of −2.5 to −3.4 m. This structure has no clear expression on either the SDB or VHR satellite images, except for a vague anomaly on two Google Earth images (24/9/2014, 29/10/2016) (Fig. 7). Moreover, the exposed portion of the submerged jetty stands proud of the seabed by < 1 m (it comprises 2 courses of stone blocks of 0.45–0.55 m thickness: (Noureddine and Mior, 2013)). This is within the vertical uncertainty of the commercial SDB, hence reducing its likelihood of detection.

The submerged southern quarter contains structures, columns, quarries, walls and pavements suggestive of an urban area. These are surrounded by linear features, originally interpreted as moles/breakwaters, but now interpreted as polder walls (Marriner et al., 2008). Some of these features, notably the walls, are distinguishable on VHR satellite imagery. Groups of structures are visible as darker features, though they cannot be clearly identified as archaeological from imagery alone (Fig. 8A). The commercial SDB picks out some of the larger features. The seaward side of the walls are defined by a clear linear edge, while the inward turning sections flanking the Bab al-Mina channel are

picked out as areas of shallow bathymetry (Fig. 8B; C). However, the deeper channel forming Bab al-Mina itself is not well-defined. Within the walls, there are hints of bathymetric variations corresponding to groups of structures (St 1006 to St1012, variously comprising dams and unidentified structures within dredge spoil: (Marriner et al., 2008; Semaan, 2016)). Although these are upstanding features, the SDB shows shallow pits (Fig. 8C). This may result from the fact that a key physical principle behind SBD is that shallow water appears light on satellite images, and deeper water is dark. Thus, unless well-constrained by control depths, dark upstanding features may be mistakenly predicted as depressions. A final feature identifiable on the SDB is a large (170 m × 75 m) shallow (<2 m deep) basin, located southwest of the submerged quarter, and which has its seaward side blocked off by a distinct linear ridge (Fig. 8C). There is no clear indication that this is artificial, and could simply be a natural seabed feature.
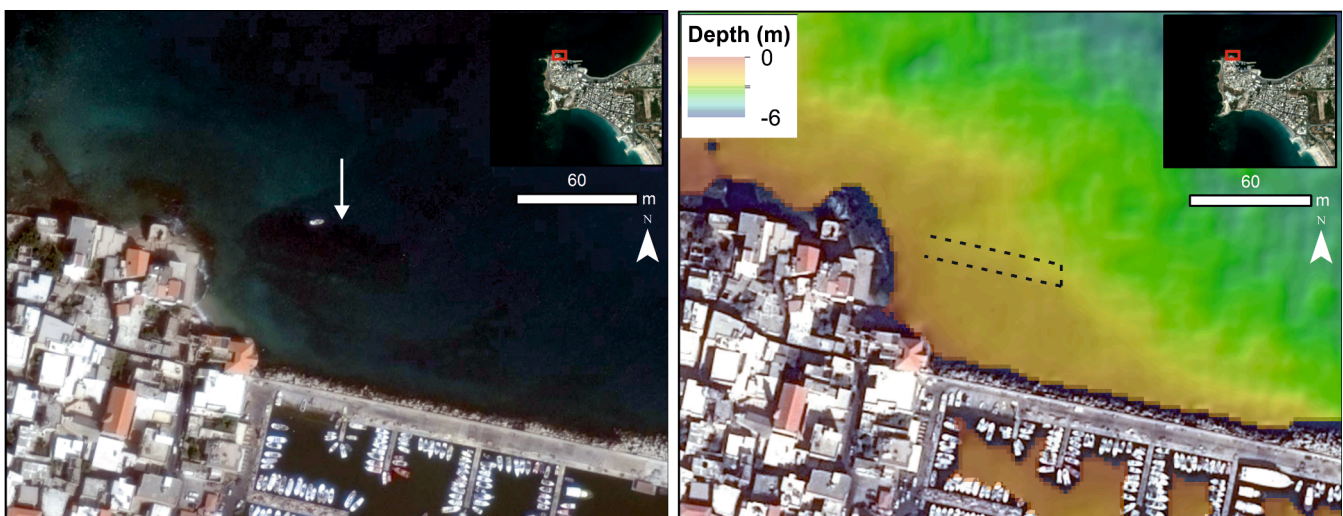


**Fig. 7.** Comparison of VHR satellite image (left: Google Earth, 24/9/2014) and commercial SDB (right) off Tyre's north harbour (see inset image for location). A faint linear anomaly (indicated by arrow) corresponds to the position of the submerged Phoenician jetty (Noureddine and Mior, 2013) but lacks surface expression on the SDB (dashed black lines show position of the jetty walls based on Noureddine and Mior, 2013: Map 1).
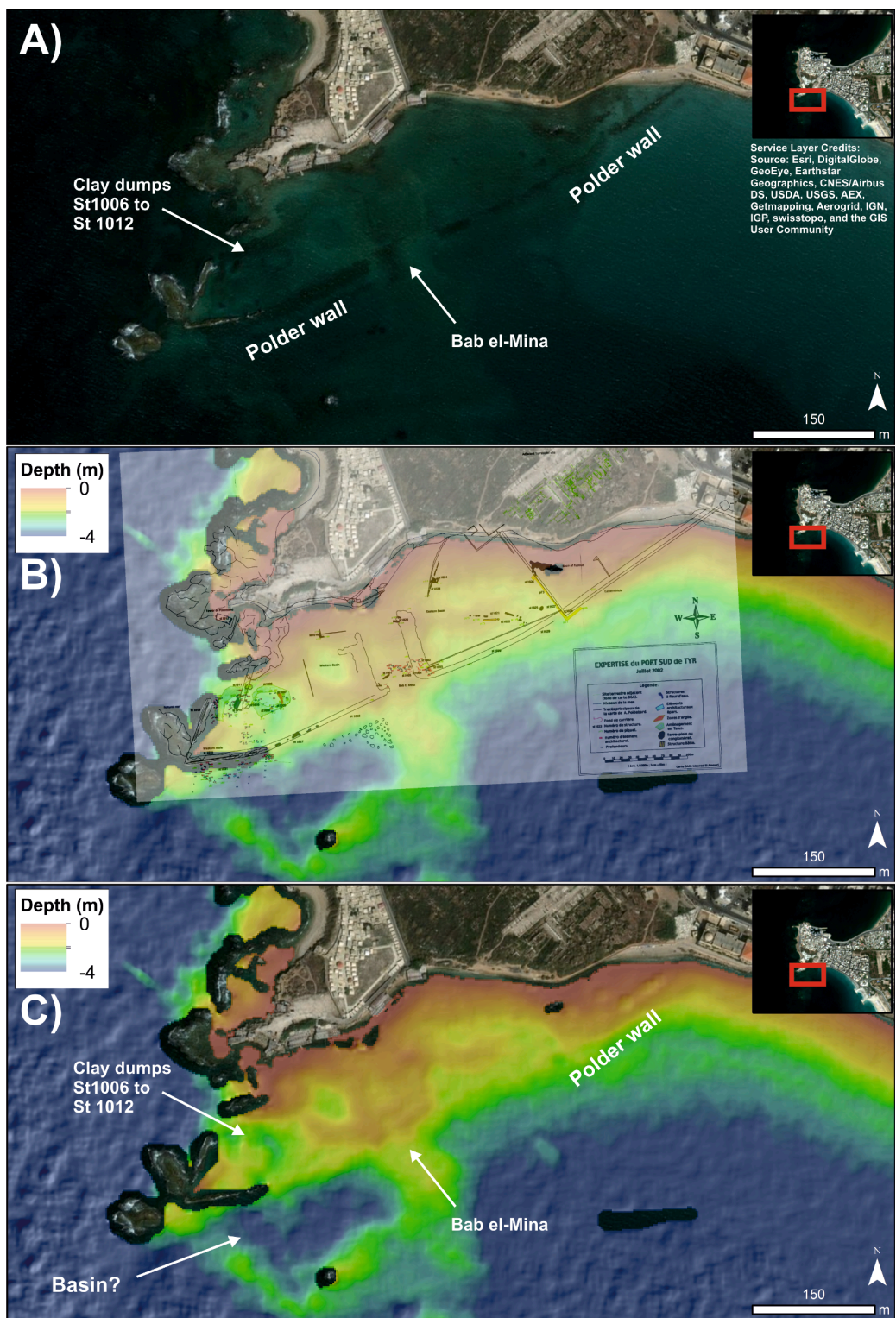
**Fig. 8.** Comparison images of the submerged urban quarter of Tyre. A) VHR satellite image; note visible archaeological features. B) archaeological plan (from Semaan, 2016: Fig 342) overlaid onto hillshaded commercial SDB). C) Hillshaded commercial SDB with features mentioned in the text indicated.

*6.2. Ras Ibn Hani*

Ras Ibn Hani lacks definitive evidence of ancient wrecks, but this may be due to a lack of survey rather than true absence of evidence (Haldane, 1993; Kampbell, 2013). Charted modern wrecks within the area of SDB coverage comprise an obstruction north of the peninsula, two wrecks (both unidentified and with few survey details) in the bay

south of the peninsula and the wreck of the SS *Megisti* (lost 1968) located ~1 km along the coast south of this bay. Neither the SDB data nor VHR satellite imagery show anomalies at any of the charted locations. However, the nature of the obstructions and the unknown wrecks (e.g. size, height) are not described in any reportage; therefore it is unclear if they theoretically should be resolvable. For the SS *Megisti*, some reports indicate that she was broken up *in situ*, hence substantial

remains on the seabed are probably low-lying or absent (Wrecksite.eu, 2020). There are no published underwater archaeological investigations from the bays at Ras Ibn Hani. However, onshore survey has recorded jetties/moles on either side of the peninsula (Carayon, 2008; Marriner et al., 2012). None of these features are visible on the SDB data (Fig. 9). For the southern bay, this is probably because these structures lie above water and may have been built over by modern structures. For the northern bay, the ancient structures are no longer visible in recent imagery and have either been removed or built over by a modern jetty (Westley et al., 2018).

## 7. Palaeo-landscape mapping

### 7.1. Tyre

The main submerged landform visible on all SDB datasets is the offshore ridge which runs discontinuously to the north and south of Tyre (Figs. S1; S2). Above-water exposures of the ridge, such as on the outer face of the peninsula, reveal it to be sandstone. Elsewhere in the Levant, similar features are found on– and offshore and are locally known as *kurkar* or *ramleh*. These are identified as fossilized beach ridges or dunes composed of cemented wind-blown sand (aeolianite) and which generally date to the Late Pleistocene and Holocene (Beydoun, 1976; Galili et al., 2007; Mauz et al., 2013). The aeolianite ridges are thus relict palaeo-landscape features and provide evidence of climate and sea-level change (Mauz et al., 2013). From a taphonomic standpoint, they can also influence archaeological preservation. Inter-ridge hollows provide locations where lower-energy alluvial silts and clays can accumulate. These sheltered alluvial/lagoonal-type landscapes may firstly have been attractive areas for occupation; secondly, the low energy nature of deposition also afforded a greater possibility for *in situ*/minimally reworked preservation and finally the ridges could act as natural breakwaters during inundation, thus limiting erosion of the archaeological evidence. A potential example of this is the submerged Neolithic village of Atlit-Yam located ~65 km to the south (Flemming et al., 2017; Galili et al., 2017, 1993). This raises the possibility that similar environments could exist in the lee of the ridges along the Tyre coastline.

In later periods, the natural shelter of these ridges has been interpreted as crucial in the development of safe anchorages and ancient harbours (Marriner et al., 2008, 2006, 2005). For Tyre, Marriner et al. (2008) speculate that satellite anchorages were located at Tell Rachideye, ~4 km southwest, because of protective offshore reefs. However,
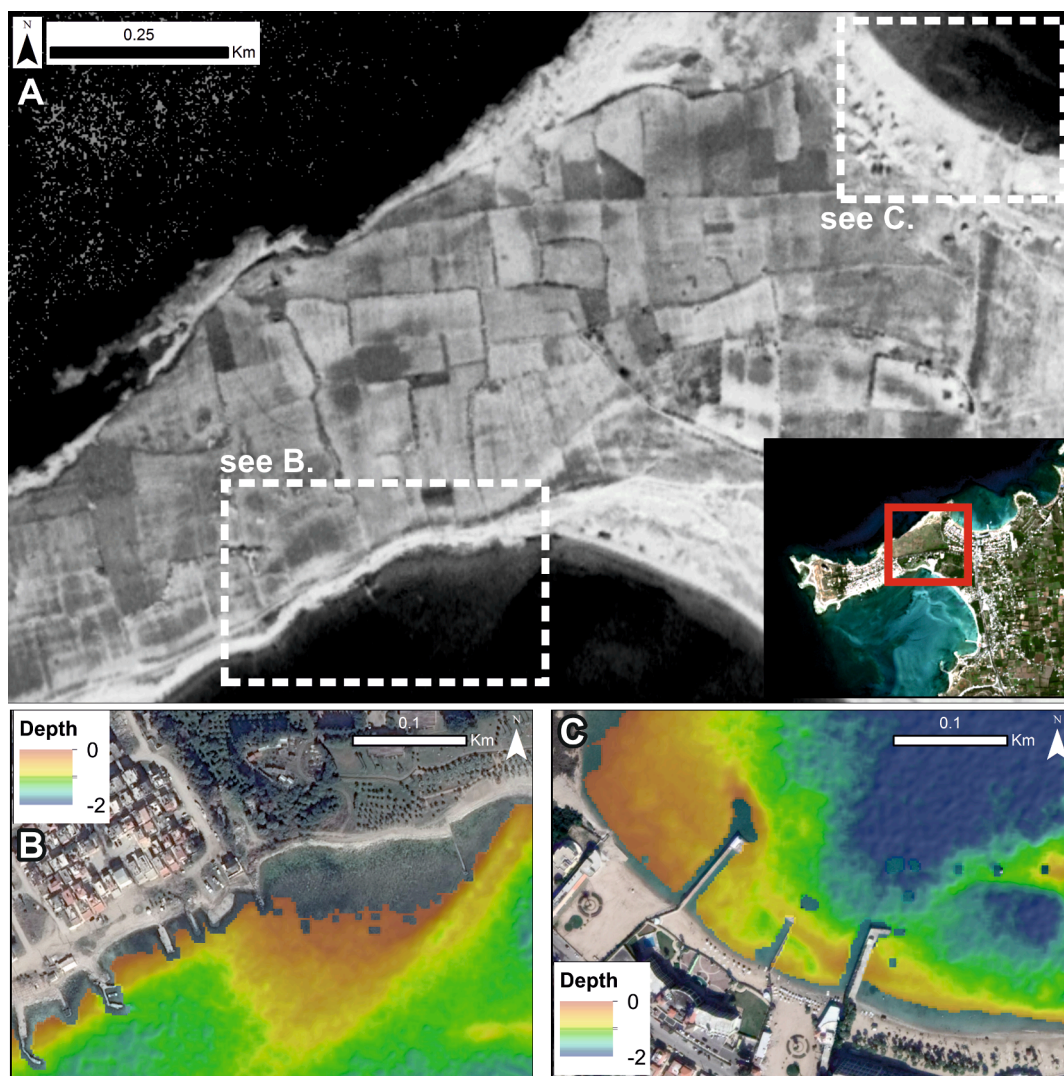


**Fig. 9.** Images for Ras Ibn Hani focussing on ancient jetties or moles. A) Corona satellite image (20/11/1968); note faint traces of jetties at locations identified by Carayon (2008) and Marriner et al. (2012). B) VHR image (Google Earth: 8/2/2014) showing location of jetties in the south bay with commercial SDB overlain. It is unclear from the imagery alone which jetties are modern, ancient or modern structures built on top of an ancient core. C) VHR image (Google Earth: 20/10/2017) showing location of jetties in the north bay with commercial SDB overlain. All jetties shown are modern, a potential ancient one seen in pre-2016 imagery has been removed.

the SDB is equivocal regarding the extension of the reefs this far south of Tyre. Both the commercial and best-performing empirical variants show that the ridges here are deeper and less prominent that their counterparts at Tyre itself (Figs. 2, S1, S2). Therefore this casts doubt on the suitability of this area as a protected anchorage. However, the extension of the ridge far to the north of Tyre demonstrates that such anchorages could be found here (see also Semaan, 2016 for discussion of the suitability of Adloun and Sarafan, located in this zone, as natural harbours).

Palaeo-geographic reconstructions based on the commercial SDB also highlight the advantages and disadvantages of these data to explore past coastal change. Fig. 10 compares SDB-based reconstructions for Tyre with those by Marriner et al. (2008: Fig. 11). The key difference is the inability of the SDB data to account for sedimentation. Thus the SDB-based reconstruction predicts Tyre to be connected to the mainland, whereas Marriner et al.'s (2008) reconstructions – based on palaeo-environmental and geological data – correctly show Tyre as an island until after 330 BC when the connecting tombolo began to form. This problem is not restricted to SDB, but use of any bathymetric surface as an analogue for the past landsurface (Westley et al., 2014). However, use of high-resolution SBD rather than low-resolution bathymetry arguably produces more representative reconstructions where sedimentation is reduced. Thus, the offshore island formed by the modern reef is

reconstructed to be much smaller between 8000 and 6000 BP if the SDB data is used (Fig. 10A). For subsequent timesteps (Fig. 10B to E), the SDB-based reconstructions suggest the island was again smaller, with its northern extremity composed of isolated reef/islets rather than the continuous peninsula suggested by Marriner et al. (2008).

An advantage of SDB is the large area which can be covered. Fig. 11 shows a palaeo-geographic reconstruction for the general area around Tyre, assuming RSL of −7 m (equivalent to ~8000–6000 BP: Marriner et al., 2008). It compares reconstructions using empirical SDB and open source low-resolution (~225 m) EMODnet bathymetry (EMODnet Digital Bathymetry, 2016). EMODnet data only provide a basic approximation of the coastline, with no expression of the offshore ridges. Both the Sentinel-2 and Landsat 8 SDB have greater detail and show better the extent of the former island of Tyre. They both also suggest a small bay/channel and another set of offshore islands/peninsulas respectively 7.7 km and 10.3 km north of Tyre. The caveats are that none of the bathymetric data can account for sedimentation - since this can vary considerably on a local-scale, and is therefore only available intermittently on a site-specific basis (e.g. Marriner et al., 2008, 2006, 2005) – and that the single RSL value used cannot account for the complexity of Holocene RSL change on the Lebanese coast where tectonic movement of individual crustal blocks can create localized vertical variation (Morhange
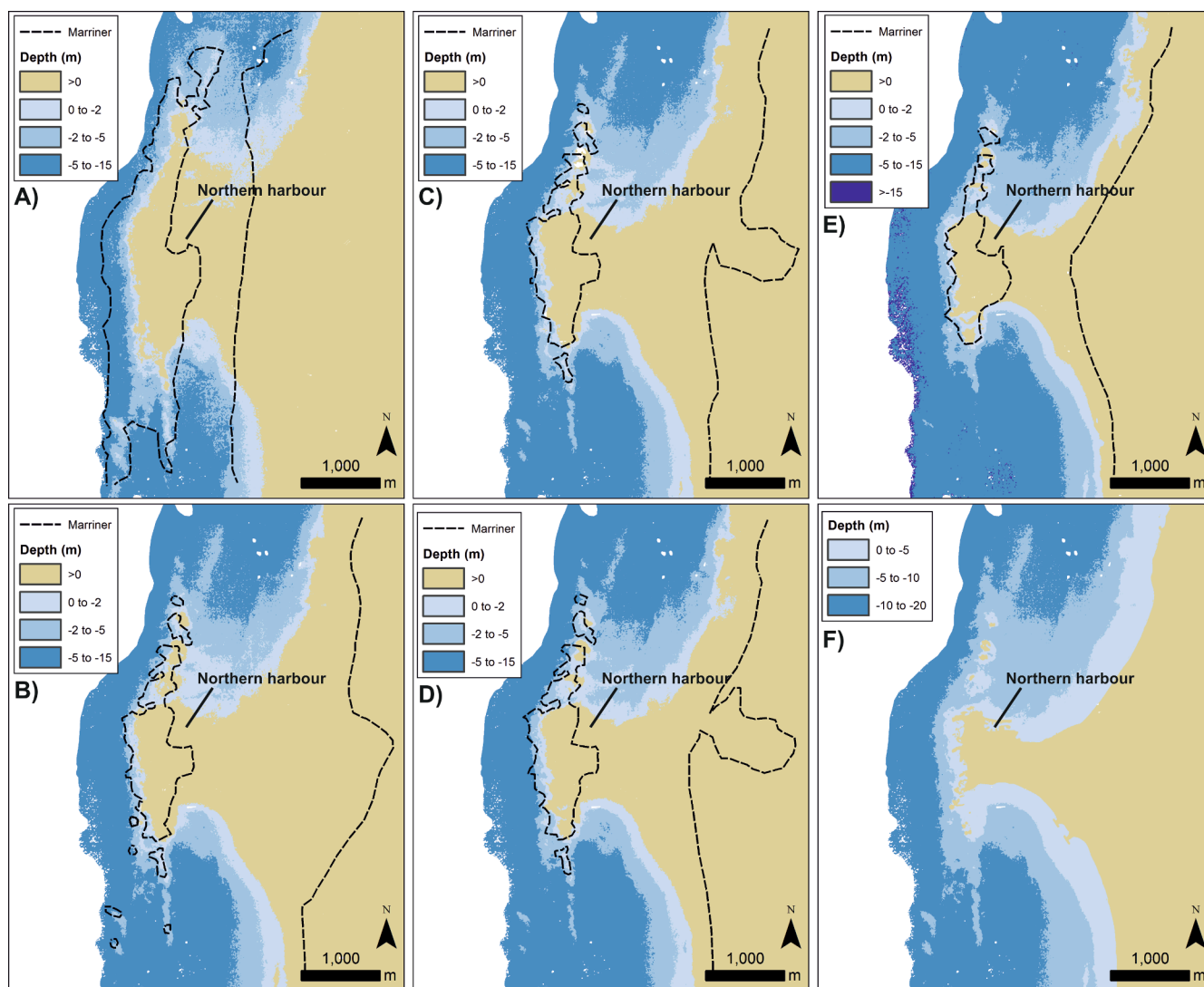


**Fig. 10.** Time-stepped palaeo-geographic reconstructions for Tyre based on commercial SDB data and RSL data from Marriner et al. (2008). Palaeo-shorelines reconstructed by Marriner et al. (2008: Fig. 11) are superimposed as dashed lines. A) 8000–6000 BP. B) 6000 BP. C) 4000 BP. D) 3000 BP. E) 330 BC. F) Present day.
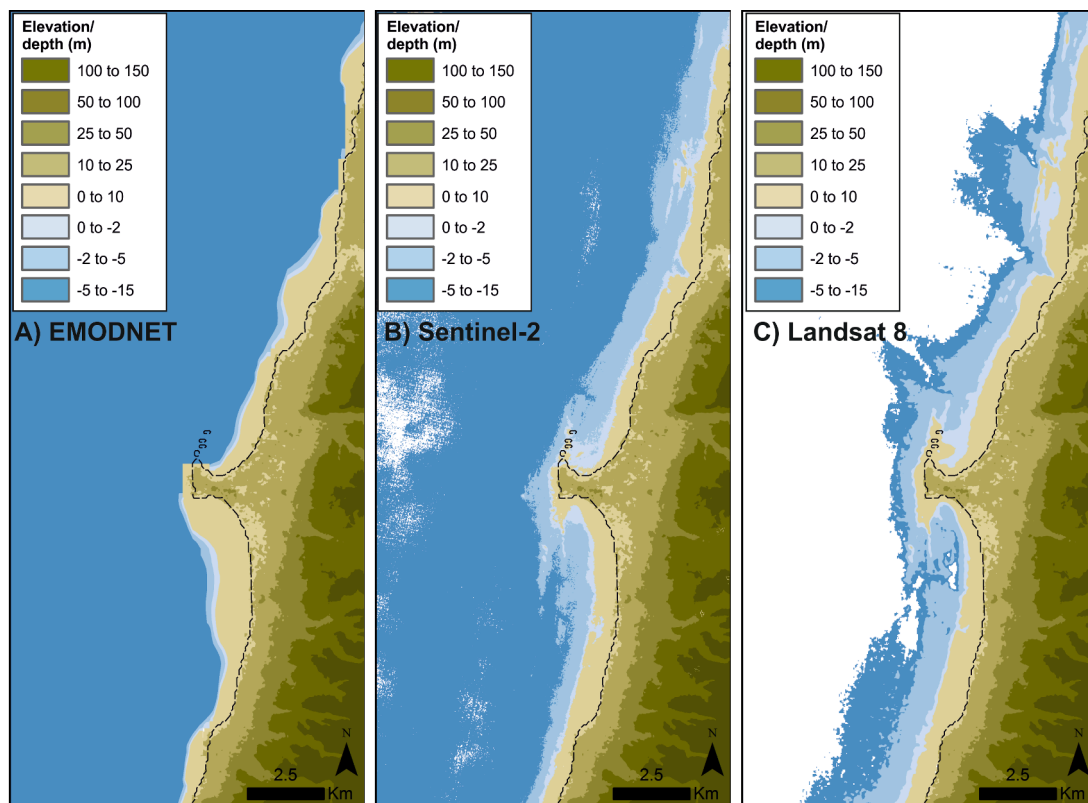
**Fig. 11.** Palaeo-geographic reconstructions for the general Tyre coastline using modern bathymetry and assuming an RSL fall of −7m (equivalent to ~8000–6000 BP: Marriner et al., 2008). A) Low-resolution EMODnet bathymetry. B) Sentinel-2 SDB (Lyzenga B2-3). C) Landsat 8 SDB (Stumpf Polynomial). Dashed line indicates modern shoreline, terrestrial digital elevation model is from the SRTM 1 arc-second dataset (Farr et al., 2007).



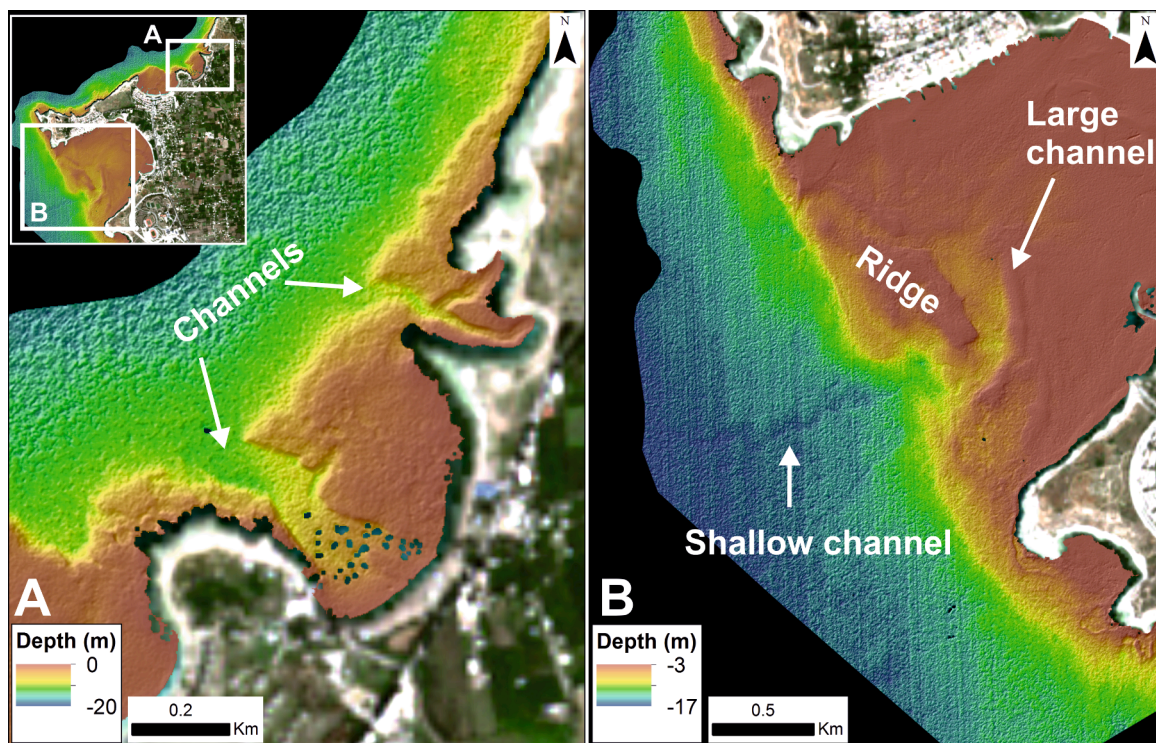**Fig. 12.** Hillshaded commerical SDB showing channel-like features at Ras Ibn Hani. A) Large and small channels at Minet el-Helu. B) Entrance to the bay south of Ras Ibn Hani showing a large channel cutting through the ridge and a faint shallow channel on the deeper seabed.

et al., 2006). Nevertheless, such reconstructions can at least be used to give first order indications of the former landscape and potentially be used as inputs into wave/wind models for harbour/anchorage suitability (e.g. Safadi, 2016).

### 7.2. Ras Ibn Hani

All SDB datasets show an extended level or gently sloping platform which fronts the modern coast (Figs. 3; S3; S4). Where the platform is well developed, and based on the commercial SDB, its seaward edge lies at a depth of c. −3 m to −5 m. This then gives way to a steeper slope or cliff whose base consistently lies at −12 m to −10 m, and transitions to a level or gently sloping seabed. This cliff and platforms potentially represent marine terraces formed by wave erosion during periods of lower RSL. It is possible that the shallow platforms are the result of modern and late Holocene processes, while the deeper cliff and terrace are from an earlier period of lower RSL. More research would however be needed to confirm this hypothesis.

Other potential features pertaining to the former landscape are channels cut into the submerged platform. These are clearest at Minet al-Helu where there is a large (350 m long by 100 m wide) channel as well as two smaller (up to 25 m wide) sinuous channels (Fig. 12A). The larger channel links to a small stream presently visible onshore (Wadi Helou: Marriner et al., 2012). However, there is no clear evidence of watercourses draining into the smaller channels. It is possible that these were diverted either as a result of natural landscape change or anthropogenic action. In the southern bay, a 400 m long by 250 m wide channel cuts through an upstanding ridge which lies at the bay mouth. There is no clear expression of a link between this channel and onshore watercourses. However, the commercial SDB data show a faint trace of a narrow sinuous and shallow (<2 m deep) channel which lies offshore of the ridge and appears to link directly to the larger channel (Fig. 12B). If so, it could represent a palaeo-channel cut when RSL was lower, and fits with the presence of a hypothesized watercourse in this bay (Marriner et al., 2012).

Fig. 13 compares commercial SDB-based reconstructions for Ras Ibn Hani with those by Marriner et al. (2012: Fig. 7). As for Tyre, the key difference is the inability of the SDB to account for sedimentation. Thus, for the lagoon timesteps (~7500–6500 BP), it predicts Ras Ibn Hani to be part of the mainland, whereas Marriner et al.'s (2012) geo-archaeological data correctly show that it was an offshore island separated by a shallow lagoon until after ~4000 BP. For earlier timesteps (pre-10500–9500 BP), the SDB and Marriner et al. (2012) reconstructions both indicate that the bays around Ras Ibn Hani were
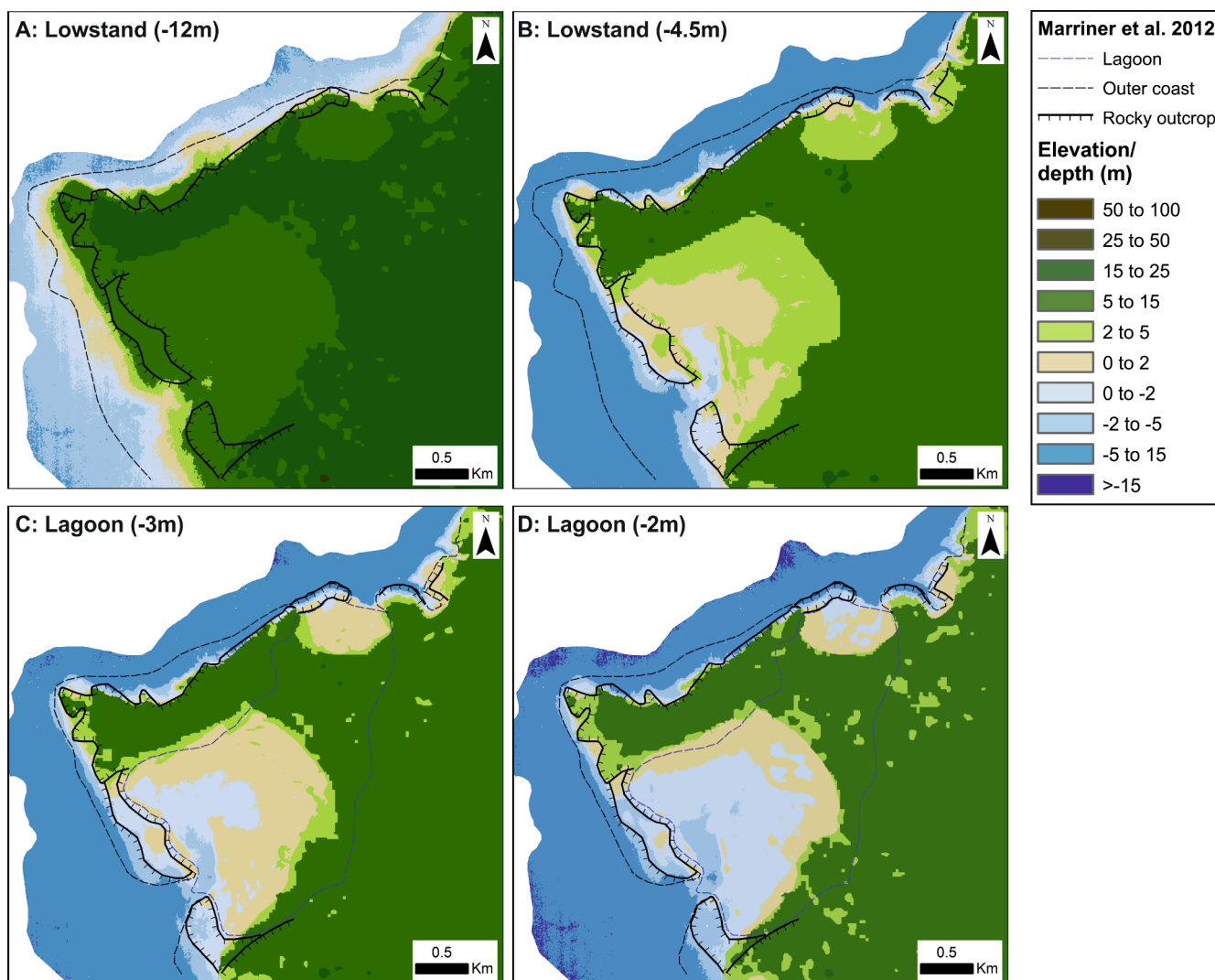


**Fig. 13.** Palaeo-geographic reconstructions for Ras Ibn Hani based on commercial SDB and RSL from Marriner et al. (2012). Palaeo-shorelines and landforms reconstructed by Marriner et al. (2012: Fig. 7) are superimposed as dashed and hatched lines. A) Undated lowstand of −12 m, coincident with the base of the submerged cliff around Ras Ibn Hani. B) Lowstand of −4.5 m, just below the depth of the lowest dated terrestrial sample from Ras Ibn Hani (10.5 to 9.9 ka cal BP: Marriner et al. 2012). C) and D) RSL of −3m and −2m respectively, coincident with the depth of lagoonal depsoits dated to c. 7.5 to 6.5 ka cal BP.

largely subaerial. As with Tyre, the high-resolution SDB also raises questions regarding elements of the past landscape. The SDB-reconstructions suggest that the rocky outcrops identified by Marriner et al. (2012) at the bay mouths are less prominent than envisaged. For the south bay, there is a clear ridge across the central part of its entrance (Fig. 13), but its connection to the peninsula is low-lying. For the north bay, the extended outcrop forming its northeastern entrance is absent. These landforms are seen as important in creating shelter which first allowed lagoon formation, and later favoured anchoring. Less prominent outcrops could suggest that the degree of shelter was somewhat reduced. While the presence of the lagoon is not debated, it does raise questions as to whether it was as large as reconstructed by Marriner et al. (2012).

Comparison can also be made between empirical SDB and low-resolution EMODnet bathymetry (Fig. 14). Two lowstand RSL positions are presented: −12 m, roughly coincident with the submerged cliff base, and −4.5 m, just below the depth of the lowest $^{14}$C-dated terrestrial deposit (∼10.5–9.9 ka cal BP: Marriner et al. (2012)). The EMODnet data provide a basic approximation of the palaeo-coastline showing only that it extended up to 1 km offshore. Conversely, the SDB show in more detail the variable flooding taking place in the south bay due to the presence of the channel and ridge. The EMODnet data also appear to greatly overestimate the extent of the former coastal plain, particularly north of Minet el-Beida. By contrast, the SDB reconstructions highlight that the area around Ras Ibn Hani was unique on this stretch of coast by having an extended coastal plain which enabled the development of shallow embayments as sea-level rose. The data also suggest that Minet el-Beida was transformed into an embayment before the bays north and south of Ras Ibn Hani. As for Tyre, the caveats are that none of the bathymetric data account for sedimentation and that there is a risk in using single RSL values for reconstruction in tectonically complex areas such as Syria (Dodonov et al., 2008; Sanlaville et al., 1997).

## 8. Discussion: Application of SDB to maritime archaeology

Accurate bathymetry is a standard core variable for maritime archaeology (Flemming, 2017; Menna et al., 2018). High-resolution bathymetry (defined here as metre- to sub-metre vertical and
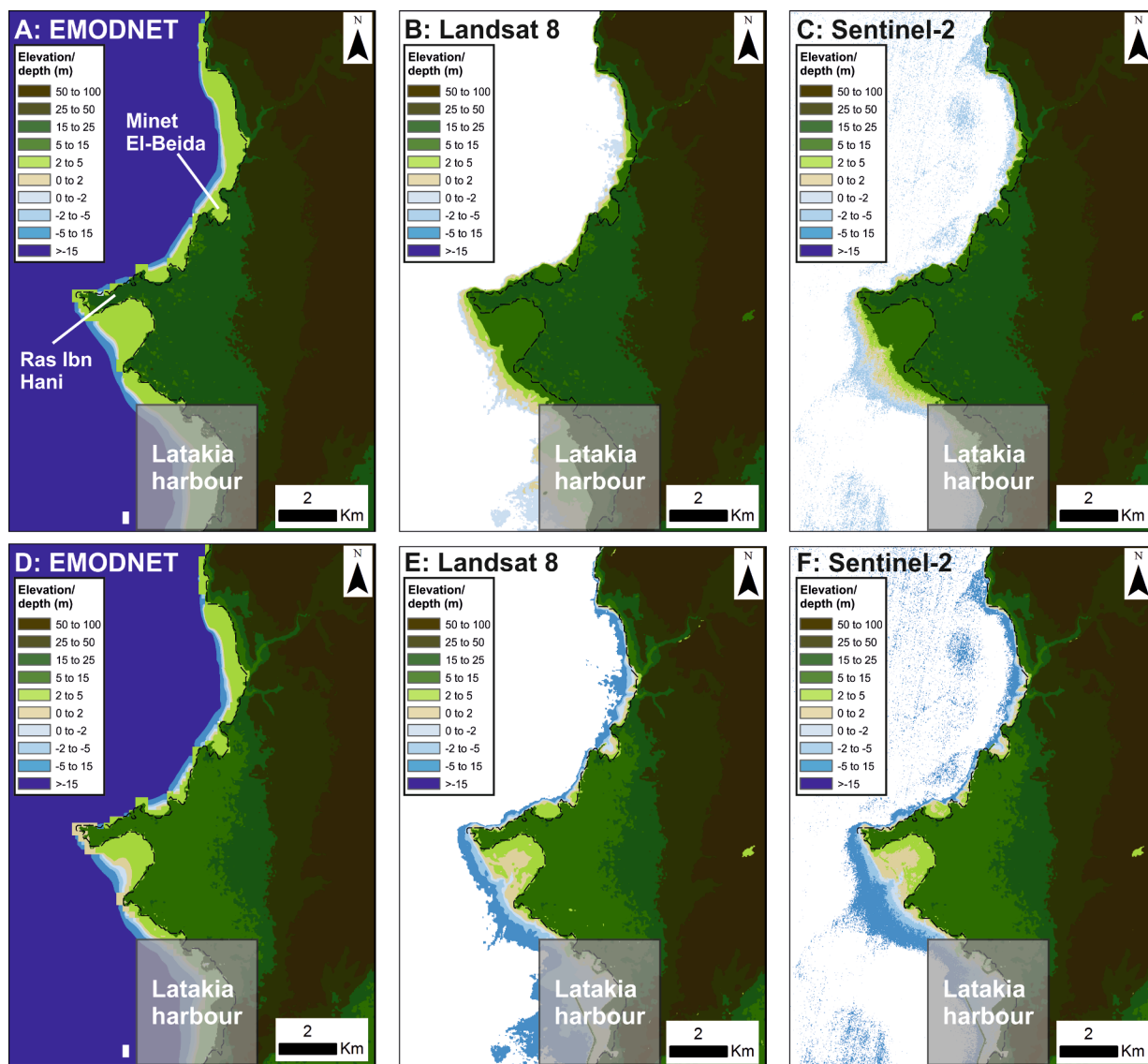


**Fig. 14.** Palaeo-geographic reconstructions for the Ras Ibn Hani area using modern bathymetry and RSL of −12 m (A to C), and −4.5 m (D to F). A and D) Low resolution EMODNET bathymetry. B and E) Landsat 8 SDB (Stumpf Exponential). C and F) Sentinel-2 SDB (Stumpf Exponential). Dashed line indicates modern shoreline, terrestrial digital elevation model is from the SRTM 1 arc-second dataset (Farr et al., 2007). Latakia harbour has been excluded because of high turbidity and extensive recent anthropogenic modification of the coast.

horizontal resolution) is particularly valuable for underwater archaeological prospection, understanding site formation processes, palaeolandscape reconstruction, assessment of archaeological potential, record enhancement, asset visualization, survey planning and repeat monitoring (Bates et al., 2011, 2013; Davis et al., 2020; Fernández-Montblanc et al., 2016; Majcher et al., 2020; Menna et al., 2018; Plets et al., 2013, 2011; Westley et al., 2019, 2011).

Whilst high-resolution data derived from swath bathymetry or airborne LiDAR surveys are increasingly available (e.g. Infomar [Ireland], Civil Hydrography Programme [UK], CoNED [USA]) this is not universal. Large tracts of the seabed remain unsurveyed, or not surveyed to modern standards (Mayer et al., 2018; Wölfl et al., 2019). Alternatively, high-resolution data may be restricted for military or commercial reasons. In these cases, archaeologists and heritage managers are reliant on the most basic level of detail from hydrographic charts (which may also be out of date) or low-resolution digital elevation models (e.g. EMODnet or GEBCO). SDB therefore seems to offer an attractive means of redressing this for shallow waters. Based on the literature, and the work presented here which shows that all tested SDB algorithms can resolve at least basic seabed morphology, it is apparent that SDB has some advantages. These are:

- **Cost:** SDB can be freely derived at spatial resolutions of 10 m to 30 m using published approaches and open access satellite imagery (Landsat 8, Sentinel-2). Notwithstanding successful application of empirical SDB to free high-resolution Google Earth imagery (Collin et al., 2014), obtaining higher resolution (<5m) SDB generally entails a cost. This is either to purchase high-resolution satellite images for self-processing or direct purchase of processed SDB from a commercial provider. Even so, the cost tends to be lower than the equivalent offshore survey as there is no need for boats, equipment, crew and fuel (Heege et al. 2017).
- **Speed:** SDB can be rapidly derived using empirical approaches for areas covering tens of km$^2$ in a matter of hours. This compares favourably to offshore survey which could require several days of acquisition and follow-up processing to cover the same area. Physics-based approaches were not directly trialled here, so the exact speed of processing is unclear, but is also likely to be faster than surveying the equivalent area directly (see also Guzinski et al., 2016; Heege et al., 2017).
- **Coverage:** shallow inshore waters are traditionally hard to survey. This is because of potential uncharted hazards and that, if conventional MBES is used, the effective swath width decreases with depth so that more survey lines (and hence more time and expense) are required. If water conditions are right, then SDB can fill this gap. In addition, satellite imagery coverage is global. Several commercial providers also now offer either off-the-shelf SDB at varying resolutions and near-global coverage, or tools which end-users can use for empirical or physics-based derivation (e.g. EOMAP, 2020; TCARTA, 2020). Therefore, data availability is not a problem.

However, SDB also has some disadvantages:

- **Effectiveness**: The maximum depth which can be resolved depends heavily on local sea and atmospheric conditions at the time of image acquisition. Thick clouds obscure the sea while atmospheric scattering requires correction. Moreover, high turbidity, sun glint and waves all reduce the effectiveness of SDB (Casal et al., 2019). Consequently, SDB will be less effective in variably turbid areas (but note attempts to use it in such conditions: Bramante et al., 2013; Caballero and Stumpf, 2020; Pe'eri et al., 2016), while changing daily weather conditions mean that there will always be some images which are unsuitable.
- **Accuracy:** the comparisons here indicate that accuracy - in terms of absolute derived depth values - can vary considerably depending on algorithm and image choices. Additional variation can also result

from the atmospheric correction and sun-glint corrections (Casal et al., 2019; Traganos et al., 2018). Moreover, for empirical approaches, any errors or biases in the depth control data could be carried over to the SDB. For instance, hydrographic chart soundings may be sparse and/or out of date. For Ras Ibn Hani test, considerable variation was evident over the shallow platform, and these errors may have been exacerbated by the lack of soundings on the available hydrographic chart. Another potential error lies in the shallow- or shoal-biased nature of hydrographic charts since they are intended for safety of navigation rather than a 'true' map of seafloor morphology (Flemming, 2017). For the tests here, this could partly explain the tendency of the open source approaches to under-predict relative to the commercial SDB. That said, the empirical tests here represent the most basic form of SDB and there have been recent methodological advances such as multi-image processing or depth control from space-based laser which improve accuracy (Caballero and Stumpf, 2020; Ma et al., 2020).

- **Approaches:** the basic empirical approaches are straightforward to implement (though some specialised knowledge is required for recent versions which employ more advanced processing), but require control data which is not always available. Moreover, even when control data is available, it can be questionable as to how well it actually reflects the seafloor morphology (see above). At present, this remains a disadvantage, but could significantly redressed in the future given the development of space-based laser depth measurements which can provide depth control at a global scale (Ma et al., 2020; Parrish et al., 2019). Physics-based approaches are harder to implement for non-specialists and require collaboration with specialist scientists (e.g. Guzinski et al. 2016) or direct purchase of processed data from a provider.

Overall, SDB is not universally applicable to all areas and archaeological questions. From a technical standpoint it is most effective where water clarity is good, and cloud-free periods are extensive so as to allow a broader choice of images. Ideally, it requires accurate and up-to-date soundings to conduct empirical derivation or validate physics-based methods. From an archaeological standpoint, the tests here and Guzinski et al. (2016) indicate that use of SDB for prospection is not ideal. No clear wreck or archaeological signatures were detected here, and while Guzinski et al. (2016) successfully imaged a large shipwreck (50 m long, up to 9 m high) using VHR (<2m) SDB, the details of this wreck were not particularly clear. Smaller, more subtle features such low-lying or partly buried wrecks and ancient harbour installations will most likely go undetected. Arguably, for a feature to appear clearly on the SDB, it would probably need to have a distinct signature on the original satellite image and therefore be visible without the need for bathymetric derivation. Thus, at present, acoustic surveys or Structure-from-Motion photogrammetry will likely remain the standard for underwater archaeological prospection and imaging.

The utility of SDB at this time lies in providing broad-scale landscape information which goes beyond low-resolution charts and DEMs. Depending on the input imagery (e.g. Landsat 8 or Sentinel-2 versus VHR satellites such as Worldview or Pleiades), it may provide lower or equivalent resolution to swath bathymetry. This level of detail is sufficient to aid in submerged landform identification (where these are exposed on the seabed surface: e.g. offshore ridges for Tyre, submerged channels for Ras Ibn Hani), planning of field surveys and palaeogeographic reconstructions. Low-resolution bathymetry is already often used for these purposes (e.g. Dean et al., 2020; Fischer et al., 2010) thus an increase in resolution would be a bonus, particularly when it could provide clearer identification of submerged relict landforms. This would be a benefit to projects which aim to identify and document geological and geomorphological evidence of submerged palaeo-landscapes (e.g. Andreou et al., 2020). Also, for palaeo-geographic reconstructions, the fact that SDB encompasses the hard-to-survey coastal strip increases its utility for creating seamless

onshore-offshore reconstructions. The main caveats are accuracy and use of modern bathymetry as an analogue of the past landscape. To offset this, SDB would be ideally used in conjunction with additional geological data (e.g. core samples, seismic profiles). Additional uses, not tested here, could include input into wave models for investigating ancient navigation and harbour suitability (e.g. Safadi, 2016) or use of repeat SDB for change detection on dynamic seabeds that have archaeological sites (e.g. Fernández-Montblanc et al., 2016; Majcher et al., 2020; Quinn and Boland, 2010).

## 9. Conclusion

Remote sensing approaches offer an attractive means of identifying, recording and monitoring archaeological sites across large study areas. However, traditional approaches based on multispectral satellite imagery are less effective in watery environments compared to on land. In theory, this could be enhanced by using SDB to extend their archaeological utility. The application and effectiveness of SDB to maritime archaeology has been tested by reference to case studies in the Eastern Mediterranean (Lebanon, Syria). This, combined with the current literature, highlights that their effectiveness for archaeological and heritage management purposes is mixed. For SDB, this primarily relates to its technical limitations such as the need for shallow clear water, variable accuracy stemming from use of different algorithms, approaches, images and pre-processing corrections (though these are being addressed by recent advances). There are also purely archaeological issues such as poor imaging of relatively small cultural features. However, SDB is useful in getting a broader sense of the underwater landscape and environmental context in which archaeological sites are located. This information can, in turn, be used for palaeo-geographic reconstructions, assessment of archaeological potential and planning field survey, with potential extensions into site formation process studies and hydrodynamic modelling. In addition, SDB has a number of key advantages, specifically cost, coverage and speed. It is cheaper than offshore survey (or entirely free), and has near-global coverage, either in terms of suitable imagery for empirical derivation or now routine availability of off-the-shelf commercial SDB. Many coastal areas with archaeological sites lack good bathymetric data. SDB therefore offers the opportunity to improve from a position of no/poor data to reasonable/good data and using this advance to gain new insights that would not otherwise have been possible. As such, SDB has a place in the maritime archaeological toolbox, but will be variably rather than universally effective depending on to local conditions and the archaeological questions being addressed.

## CRediT authorship contribution statement

**Kieran Westley:** Conceptualization, Methodology, Investigation, Writing - original draft, Writing - review & editing, Funding acquisition.

## Appendix A. Supplementary data

Supplementary data to this article can be found online at https://doi.org/10.1016/j.jasrep.2021.103030.

## References

Almar, R., Bergsma, E.W.J., Gawehn, M.A., Aarninkhof, S.G.J., Benshila, R., 2020. High-frequency Temporal Wave-pattern Reconstruction from a Few Satellite Images: A New Method towards Estimating Regional Bathymetry. J. Coast. Res. 95, 996. https://doi.org/10.2112/SI95-194.1.

Andreou, G., Blue, L., Breen, C., Safadi, C.E., Huigens, H.O., Nikolaus, J., Ortiz-Vazquez, R., Westley, K., 2020. Maritime endangered archaeology of the Middle East and North Africa: the MarEA project. Antiquity 94, e36. https://doi.org/10.15184/aqy.2020.196.

Bates, C.R., Lawrence, M., Dean, M., Robertson, P., 2011. Geophysical Methods for Wreck-Site Monitoring: The Rapid Archaeological Site Surveying and Evaluation (RASSE) programme. Int. J. Naut. Archaeol. 40, 404–416. https://doi.org/10.1111/j.1095-9270.2010.00298.x.

Bates, M.R., Nayling, N., Bates, R., Dawson, S., Huws, D., Wickham-Jones, C., 2013. A Multi-disciplinary Approach to the Archaeological Investigation of a Bedrock-Dominated Shallow-Marine Landscape: An example from the Bay of Firth, Orkney. UK. Int. J. Naut. Archaeol. 42, 24–43. https://doi.org/10.1111/j.1095-9270.2012.00360.x.

Beydoun, Z.R., 1976. Observations on geomorphology, transportation and distribution of sediments in western Lebanon and its continental shelf and slope regions. Mar. Geol. 21 (4), 311–324. https://doi.org/10.1016/0025-3227(76)90013-X.

Bramante, J.F., Raju, D.K., Sin, T.M., 2013. Multispectral derivation of bathymetry in Singapore's shallow, turbid waters. Int. J. Remote Sens. 34 (6), 2070–2088. https://doi.org/10.1080/01431161.2012.734934.

Caballero, I., Stumpf, R.P., 2020. Towards routine mapping of shallow bathymetry in environments with variable turbidity: Contribution of sentinel-2A/B satellites mission. Remote Sens. 12, 451. https://doi.org/10.3390/rs12030451.

Cahalane, C., Magee, A., Monteys, X., Casal, G., Hanafin, J., Harris, P., 2019. A comparison of Landsat 8, RapidEye and Pleiades products for improving empirical predictions of satellite-derived bathymetry. Remote Sens. Environ. 233, 111414. https://doi.org/10.1016/j.rse.2019.111414.

Carayon, N., 2008. Les Ports Pheniciens et Puniques. Geomorphologie et Infrastructure. PhD Thesis. Universite Strasbourg II – Marc Bloch.

Casal, G., Monteys, X., Hedley, J., Harris, P., Cahalane, C., McCarthy, T., 2019. Assessment of empirical algorithms for bathymetry extraction using Sentinel-2 data. Int. J. Remote Sens. 40 (8), 2855–2879. https://doi.org/10.1080/01431161.2018.1533660.

Collin, A., Nadaoka, K., Nakamura, T., 2014. Mapping VHR water depth, seabed and land cover using google earth data. ISPRS Int. J. Geo-Information 3, 1157–1179. https://doi.org/10.3390/ijgi3041157.

Cuca, B., Hadjimitsis, D.G., 2017. Space technology meets policy: An overview of Earth Observation sensors for monitoring of cultural landscapes within policy framework for Cultural Heritage. J. Archaeol. Sci. Reports 14, 727–733. https://doi.org/10.1016/j.jasrep.2017.05.001.

Da Silveira, C.B.L., Strenzel, G.M.R., Maida, M., Araujo, T.C.M., Ferreira, B.P., 2020. Multiresolution Satellite-Derived Bathymetry in Shallow Coral Reefs: Improving Linear Algorithms with Geographical Analysis. J. Coast. Res. 36, 1247–1265. https://doi.org/10.2112/JCOASTRES-D-19-00029.1.

Davis, D.S., Buffa, D.C., Wrobleski, A.C., 2020. Assessing the Utility of Open-Access Bathymetric Data for Shipwreck Detection in the United States. Heritage 3, 364–383. https://doi.org/10.3390/heritage3020022.

Dean, S., Pappalardo, M., Boschian, G., Spada, G., Forenbaher, S., Juračić, M., Felja, I., Radić, D., Miracle, P.T., 2020. Human adaptation to changing coastal landscapes in the Eastern Adriatic: Evidence from Vela Spila cave, Croatia. Quaternary Sci. Rev. 244, 106503. https://doi.org/10.1016/j.quascirev.2020.106503.

Dekker, A.G., Phinn, S.R., Anstee, J., Bissett, P., Brando, V.E., Casey, B., Fearns, P., Hedley, J., Klonowski, W., Lee, Z.P., Lynch, M., Lyons, M., Mobley, C., Roelfsema, C., 2011. Intercomparison of shallow water bathymetry, hydro-optics, and benthos mapping techniques in Australian and Caribbean coastal environments. Limnol. Oceanogr. Methods 9 (9), 396–425. https://doi.org/10.4319/lom.2011.9.396.

Deroin, J.-P., Kheir, R.B., Abdallah, C., 2017. Geoarchaeological remote sensing survey for cultural heritage management. Case study from Byblos (Jbail, Lebanon). J. Cult. Herit. 23, 37–43. https://doi.org/10.1016/j.culher.2016.04.014.

Dierssen, H.M., Theberge, A.E., 2016. Bathymetry: Assessment. Encycl. Nat. Resour. Water 629–636. https://doi.org/10.1081/e-enrw-120048588.

Dierssen, H.M., Zimmerman, R.C., Leathers, R.A., Downes, T.V., Davis, C.O., 2003. Ocean color remote sensing of seagrass and bathymetry in the Bahamas Banks by high-resolution airborne imagery. Limnol. Oceanogr. 48 (1part2), 444–455. https://doi.org/10.4319/lo.2003.48.1_part_2.0444.

Dodonov, A.E., Trifonov, V.G., Ivanova, T.P., Kuznetsov, V.Y., Maksimov, F.E., Bachmanov, D.M., Sadchikova, T.A., Simakova, A.N., Minini, H., Al-Kafri, A.-M., Ali, O., 2008. Late Quaternary marine terraces in the Mediterranean coastal area of Syria: Geochronology and neotectonics. Quat. Int. 190 (1), 158–170. https://doi.org/10.1016/j.quaint.2008.02.008.

EMODnet Digital Bathymetry, 2016. DTM 2016–09-30 publication. Marine Information Service. https://doi.org/10.12770/c7b53704-999d-4721-b1 a3-04ec60c87238.

EOMAP, 2020. EOMAP Satellite Derived Bathymetry [WWW Document]. accessed 1.15.20. https://www.eomap.com/services/bathymetry/.

Farr, T.G., Rosen, P.A., Caro, E., Crippen, R., Duren, R., Hensley, S., Kobrick, M., Paller, M., Rodriguez, E., Roth, L., Seal, D., Shaffer, S., Shimada, J., Umland, J., Werner, M., Oskin, M., Burbank, D., Alsdorf, D.E., 2007. The shuttle radar topography mission. Rev. Geophys. 45, RG2004. https://doi.org/10.1029/2005RG000183.

Favoretto, F., Morel, Y., Waddington, A., Lopez-Calderon, J., Cadena-Roa, M., Blanco-Jarvio, A., 2017. Testing of the 4SM method in the gulf of California suggests field

data are not needed to derive satellite bathymetry. Sensors 17, 1–23. https://doi.org/10.3390/s17102248.

Fernández-Montblanc, T., Quinn, R., Izquierdo, A., Bethencourt, M., 2016. Evolution of a Shallow Water Wave-Dominated Shipwreck Site: Fougueux (1805), Gulf of Cadiz. Geoarchaeology 31 (6), 487–505. https://doi.org/10.1002/gea.2016.31.issue-610.1002/gea.21565.

Fischer, E.C., Bar-Matthews, M., Jeradino, A., Marean, C.W., 2010. Middle and Late Pleistocene paleoscape modeling along the southern coast of South Africa. Quaternary Sci. Rev. 29, 1382–1398. https://doi.org/10.1016/j.quascirev.2010.01.015.

Flemming, N.C., 2017. Standard core variables for continental shelf prehistoric research and their availability. In: Flemming, N.C., Harff, J., Moura, D., Burgess, A., Bailey, G. (Eds.), Submerged Landscapes of the European Continental Shelf: Quaternary Paleoenvironments. Wiley, pp. 83–102.

Flemming, N.C., Harff, J., Moura, D., 2017. Non-cultural processes of site formation, preservation and destruction. In: Flemming, N.C., Harff, J., Moura, D., Burgess, A., Bailey, G. (Eds.), Submerged Landscapes of the European Continental Shelf: Quaternary Paleoenvironments. Wiley, pp. 51–82.

Galili, E., Nir, Y., Vachtman, D., Mart, Y., 2017. In: Submerged Landscapes of the European Continental Shelf: Quaternary Paleoenvironments. John Wiley & Sons, Ltd, Oxford, UK, pp. 377–403. https://doi.org/10.1002/9781118927823.ch14.

Galili, E., Weinstein-Evron, M., Hershkovitz, I., Gopher, A., Kislev, M., Lernau, O., Kolska-Horwitz, L., Lernaut, H., 1993. Atlit-Yam: A Prehistoric Site on the Sea Floor off the Israeli Coast. J. F. Archaeol. 20 (2), 133–157.

Galili, E., Zviely, D., Ronen, A., Mienis, H.K., 2007. Beach deposits of MIS 5e high sea stand as indicators for tectonic stability of the Carmel coastal plain. Israel. Quat. Sci. Rev. 26 (19-21), 2544–2557. https://doi.org/10.1016/j.quascirev.2007.06.027.

Gao, J., 2009. Bathymetric mapping by means of remote sensing: Methods, accuracy and limitations. Prog. Phys. Geogr. 33 (1), 103–116. https://doi.org/10.1177/0309133309105657.

Guzinski, R., Spondylis, E., Michalis, M., Tusa, S., Brancato, G., Minno, L., Hansen, L.B., 2016. Exploring the utility of bathymetry maps derived with multispectral satellite observations in the field of underwater archaeology. Open Archaeol. 2, 243–263. https://doi.org/10.1515/opar-2016-0018.

Haldane, D., 1993. At the Crossroads of History: Nautical Archaeology in Syria. Inst. Naut. Archaeol. Quaterly 20, 7–11.

Hamylton, S.M., Hedley, J.D., Beaman, R.J., 2015. Derivation of high-resolution bathymetry from multispectral satellite imagery: A comparison of empirical and optimisation methods through geographical error analysis. Remote Sens. 7, 16257–16273. https://doi.org/10.3390/rs71215829.

Heege, T., Hartman, K., Wettle, M., 2017. Effective Surveying Tool for Shallow-water Zones. Satellite-derived bathymetry, Hydro Int.

Hodúl, M., Chénier, R., Faucher, M.-A., Ahola, R., Knudby, A., Bird, S., 2020. Photogrammetric Bathymetry for the Canadian Arctic. Mar. Geod. 43 (1), 23–43. https://doi.org/10.1080/01490419.2019.1685030.

Hritz, C., 2014. Contributions of GIS and Satellite-based Remote Sensing to Landscape Archaeology in the Middle East. J. Archaeol. Res. 22 (3), 229–276. https://doi.org/10.1007/s10814-013-9072-2.

IHO, 2016. IHC-IOC GEBCO Cookbook. IHO Public. ed. International Hydrographic Organization. https://doi.org/10.1109/C-M.1971.216840.

Kampbell, S.M., 2013. Shipwrecks of the Syrian coast. Int. J. Naut. Archaeol. 42 (2), 419–425. https://doi.org/10.1111/ijna.2013.42.issue-210.1111/1095-9270.12004.

Lecours, V., Dolan, M.F.J., Micallef, A., Lucieer, V.L., 2016. A review of marine geomorphometry, the quantitative study of the seafloor. Hydrol. Earth Syst. Sci. 20, 3207–3244. https://doi.org/10.5194/hess-20-3207-2016.

Lecours, V., Lucieer, V.L., Dolan, M.F.J., Micallef, A., 2018. Recent and future trends in Marine geomorphometry, in: Proceedings of the Geomorphometry 2018. Boulder, CO., USA, pp. 1–4.

Lyzenga, D.R., 1978. Passive remote sensing techniques for mapping water depth and bottom features. Appl. Opt. 17, 379–383. https://doi.org/10.1364/ao.17.000379.

Ma, Y., Xu, n., Liu, Z., Yang, B., Yang, F., Wang, X.H., Li, S., 2020. Satellite-derived bathymetry using the ICESat-2 lidar and Sentinel-2 imagery datasets. Remote Sens. Environ. 250, 112047. https://doi.org/10.1016/j.rse.2020.112047.

Majcher, J., Plets, R., Quinn, R., 2020. Residual relief modelling: digital elevation enhancement for shipwreck site characterisation. Archaeol. Anthropol. Sci. 12, 122. https://doi.org/10.1007/s12520-020-01082-6.

Majcher, J., Quinn, R., Plets, R., Coughlan, M., McGonigle, C., Sacchetti, F., Westley, K., 2021. Spatial and temporal variability in geomorphic change at tidally influenced shipwreck sites: The use of time-lapse multibeam data for the assessment of site formation processes. Geoarchaeology 36 (3), 429–454. https://doi.org/10.1002/gea.v36.310.1002/gea.21840.

Marriner, N., Goiran, J.-P., Geyer, B., Matoïan, V., al-Maqdissi, M., Leconte, M., Carbonel, P., 2012. Ancient harbors and Holocene morphogenesis of the Ras Ibn Hani peninsula (Syria). Quat. Res. 78 (1), 35–49. https://doi.org/10.1016/j.yqres.2012.03.005.

Marriner, N., Morhange, C., Boudagher-Fadel, M., Bourcier, M., Carbonel, P., 2005. Geoarchaeology of Tyre's ancient northern harbour. Phoenicia. J. Archaeol. Sci. 32 (9), 1302–1327. https://doi.org/10.1016/j.jas.2005.03.019.

Marriner, N., Morhange, C., Carayon, N., 2008. Ancient Tyre and its harbours: 5000 years of human-environment interactions. J. Archaeol. Sci. 35 (5), 1281–1310. https://doi.org/10.1016/j.jas.2007.09.003.

Marriner, N., Morhange, C., Doumet-Serhal, C., 2006. Geoarchaeology of Sidon's ancient harbours. Phoenicia. J. Archaeol. Sci. 33 (11), 1514–1535. https://doi.org/10.1016/j.jas.2006.02.004.

Mauz, B., Hijma, M.P., Amorosi, A., Porat, N., Galili, E., Bloemendal, J., 2013. Aeolian beach ridges and their significance for climate and sea level: Concept and insight

from the Levant coast (East Mediterranean). Earth-Science Rev. 121, 31–54. https://doi.org/10.1016/j.earscirev.2013.03.003.

Mayer, L., Jakobsson, M., Allen, G., Dorschel, B., Falconer, R., Ferrini, V., Lamarche, G., Snaith, H., Weatherall, P., 2018. The Nippon Foundation—GEBCO Seabed 2030 Project: The Quest to See the World's Oceans Completely Mapped by 2030. Geosciences 8, 63. https://doi.org/10.3390/geosciences8020063.

Menna, F., Agrafiotis, P., Georgopoulos, A., 2018. State of the art and applications in archaeological underwater 3D recording and mapping. J. Cult. Herit. 33, 231–248. https://doi.org/10.1016/j.culher.2018.02.017.

Monteys, X., Harris, P., Caloca, S., Cahalane, C., 2015. Spatial prediction of coastal bathymetry based on multispectral satellite imagery and multibeam data. Remote Sens. 7, 13782–13806. https://doi.org/10.3390/rs71013782.

Morhange, C., Pirazzoli, P.A., Marriner, N., Montaggioni, L.F., Nammour, T., 2006. Late Holocene relative sea-level changes in Lebanon, Eastern Mediterranean. Mar. Geol. 230 (1-2), 99–114. https://doi.org/10.1016/j.margeo.2006.04.003.

Noureddine, I., 2010. New light on the Phoenician harbor at Tyre. Near East. Archaeol. 73 (2-3), 176–181.

Noureddine, I., Mior, A., 2013. Archaeological survey of the phoenician harbour at Tyre. Lebanon, Report for the Honor Frost Foundation.

Pacheco, A., Horta, J., LoureiroFerreira,, C., 2015. Retrieval of nearshore bathymetry from Landsat 8 images: A tool for coastal monitoring in shallow waters. Remote Sens. Environ. 159, 102–116. https://doi.org/10.1016/j.rse.2014.12.004.

Parcak, Sarah, 2007. Satellite Remote Sensing Methods for Monitoring Archaeological Tells in the Middle East. J. F. Archaeol. 32 (1), 65–81. https://doi.org/10.1179/009346907791071773.

Parrish, C.E., Magruder, L.A., Neuenschwander, A.L., Forfinski-Sarkozi, N., Alonzo, M., Jasinski, M., 2019. Validation of ICESat-2 ATLAS Bathymetry and Analysis of ATLAS's Bathymetric Mapping Performance. Remote Sens. 11, 1634. https://doi.org/10.3390/rs11141634.

Pe'eri, Shachak, Madore, Brian, Nyberg, John, Snyder, Leland, Parrish, Christopher, Smith, Shep, 2016. Identifying Bathymetric Differences over Alaska's North Slope using a Satellite-derived Bathymetry Multi-temporal Approach. J. Coast. Res. 76, 56–63. https://doi.org/10.2112/SI76-006.

Philip, G., Donoghue, D., Beck, A., Galiatsatos, N., 2002. CORONA satellite photography: An archaeological application from the Middle East. Antiquity 76 (291), 109–118. https://doi.org/10.1017/S0003598X00089869.

Pike, S., Traganos, D., Poursanidis, D., Williams, J., Medcalf, K., Reinartz, P., Chrysoulakis, N., 2019. Leveraging Commercial High-Resolution Multispectral Satellite and Multibeam Sonar Data to Estimate Bathymetry: The Case Study of the Caribbean Sea. Remote Sens. 11, 1830. https://doi.org/10.3390/rs11151830.

Plets, R., Dix, J., Bates, C., 2013. Marine Geophysics Data Acquisition, Processing and Interpretation. Guidance notes. English Herit. 1–92.

Plets, R., Quinn, R., Forsythe, W., Westley, K., Bell, T., Benetti, S., McGrath, F., Robinson, R., 2011. Using Multibeam Echo-Sounder Data to Identify Shipwreck Sites: Archaeological assessment of the Joint Irish Bathymetric Survey data. Int. J. Naut. Archaeol. 40, 87–98. https://doi.org/10.1111/j.1095-9270.2010.00271.x.

Poursanidis, D., Traganos, D., Chrysoulakis, N., Reinartz, P., 2019. Cubesats allow high spatiotemporal estimates of satellite-derived bathymetry. Remote Sens. 11, 1299. https://doi.org/10.3390/rs11111299.

Quinn, Rory, Boland, Donal, 2010. The role of time-lapse bathymetric surveys in assessing morphological change at shipwreck sites. J. Archaeol. Sci. 37 (11), 2938–2946. https://doi.org/10.1016/j.jas.2010.07.005.

Rayne, L., Bradbury, J., Mattingly, D., Philip, G., Bewley, R., Wilson, A., 2017. From Above and on the Ground: Geospatial Methods for Recording Endangered Archaeology in the Middle East and North Africa. Geosciences 7, 100. https://doi.org/10.3390/geosciences7040100.

Rayne, L., Gatto, M.C., Abdulaati, L., Al-Haddad, M., Sterry, M., Sheldrick, N., Mattingly, D., 2020. Detecting Change at Archaeological Sites in North Africa Using Open-Source Satellite Imagery. Remote Sens. 12, 3694. https://doi.org/10.3390/rs12223694.

Safadi, S., 2016. Wind and wave modelling for the evaluation of the maritime accessibility and protection afforded by ancient harbours. J. Archaeol. Sci. Reports 5, 348–360. https://doi.org/10.1016/j.jasrep.2015.12.004.

Sagawa, Tatsuyuki, Yamashita, Yuta, Okumura, Toshio, Yamanokuchi, Tsutomu, 2019. Satellite derived bathymetry using machine learning and multi-temporal satellite images. Remote Sens. 11 (10), 1155. https://doi.org/10.3390/rs11101155.

Salameh, E., Frappart, F., Almar, R., Baptista, P., Heygster, G., Lubac, B., Raucoules, D., Almeida, L.P., Bergsma, E.W.J., Capo, S., De Michele, M.D., Idier, D., Li, Z., Marieu, V., Poupardin, A., Silva, P.A., Turki, I., Laignel, B., 2019. Monitoring Beach Topography and Nearshore Bathymetry Using Spaceborne Remote Sensing: A Review. Remote Sens. 11, 2212. https://doi.org/10.3390/rs11192212.

Sanlaville, P., Dalongeville, R., Bernert, P., Evin, J., 1997. The Syrian Coast : A Model of Holocene Coastal Evolution. J. Coast. Res. 13, 385–396.

Seco Alvarez, M., 2012. Marine archaeological intervention on a looted shipwreck a few kilometres offshore Tyre 2006-2010., in: L'Histoire de Tyr Au Temoignage de l'archeologie. Actes Du Seminaires International, Tyr 2011. Bulletin d'archéologie et d'architecture Libanaises, pp. 79–94.

Semaan, L., 2016. Desk based assessment of maritime archaeological sites on the Lebanese coast. Report prepared for the Honor Frost Foundation.

Stumpf, Richard P., Holderied, Kristine, Sinclair, Mark, 2003. Determination of water depth with high-resolution satellite imagery over variable bottom types. Limnol. Oceanogr. 48 (1part2), 547–556. https://doi.org/10.4319/lo.2003.48.1_part_2.0547.

TCARTA, 2020. TCARTA Satellite Derived Bathymetry [WWW Document]. accessed 1.15.20. https://www.tcarta.com/satellite-derived-bathymetry.

Tempfli, K., Huurneman, G.C., Bakker, W.H., Janssen, L.L.F., Feringa, W.F., Gieske, A.S. M., Grabmaier, K.A., Hecker, C.A., Horn, J.A., Kerle, N., van der Meer, F.D., Parodi, G.N., Pohl, C., Reeves, C.V., van Ruitenbeek, F.J.A., Schetselaar, E.M., Weir, M.J.C., Westinga, E., Woldai, T., 2009. Principles of remote sensing : an introductory textbook. International Institute for Geo-Information Science and Earth Observation.

Traganos, D., Poursanidis, D., Aggarwal, B., Chrysoulakis, N., Reinartz, P., 2018. Estimating satellite-derived bathymetry (SDB) with the Google Earth Engine and sentinel-2. Remote Sens. 10, 859. https://doi.org/10.3390/rs10060859.

Vanhellemont, Q., 2018. ACOLITE (v 20180925.0) [WWW Document]. URL https:// odnature.naturalsciences.be/remsem/software-and-data/acolite (accessed 10.1.18).

Vanhellemont, Q., Ruddick, K., 2018. Atmospheric correction of metre-scale optical satellite data for inland and coastal water applications. Remote Sens. Environ. 216, 586–597. https://doi.org/10.1016/j.rse.2018.07.015.

Watts, A.B., Tozer, B., Harper, H., Boston, B., Shillington, D.J., Dunn, R., 2020. Evaluation of Shipboard and Satellite-Derived Bathymetry and Gravity Data Over Seamounts in the Northwest Pacific Ocean. J. Geophys. Res. Solid Earth 125.

Westley, K., Carayon, N., Breen, C., Blue, L., 2018. Benchmarking the Maritime Cultural Heritage of Syria. Unpublished report prepared for the Honor Frost Foundation.

Westley, K., Plets, R., Quinn, R., 2014. Holocene Paleo-Geographic Reconstructions of the Ramore Head Area, Northern Ireland, Using Geophysical and Geotechnical Data: Paleo-Landscape Mapping and Archaeological Implications. Geoarchaeology 29, 411–430. https://doi.org/10.1002/gea.21489.

Westley, K., Plets, R., Quinn, R., McGonigle, C., Sacchetti, F., Dale, M., McNeary, R., Clements, A., 2019. Optimising protocols for high-definition imaging of historic shipwrecks using multibeam echosounder. Archaeol. Anthropol. Sci. 11, 3629–3654. https://doi.org/10.1007/s12520-019-00831-6.

Westley, K., Quinn, R., Forsythe, W., Plets, R., Bell, T., Benetti, S., McGrath, F., Robinson, R., 2011. Mapping Submerged Landscapes Using Multibeam Bathymetric Data: A case study from the north coast of Ireland. Int. J. Naut. Archaeol. 40, 99–112. https://doi.org/10.1111/j.1095-9270.2010.00272.x.

Wölfl, A.-C., Snaith, H., Amirebrahimi, S., Devey, C.W., Dorschel, B., Ferrini, V., Huvenne, V.A.I., Jakobsson, M., Jencks, J., Johnston, G., Lamarche, G., Mayer, L., Millar, D., Pedersen, T.H., Picard, K., Reitz, A., Schmitt, T., Visbeck, M., Weatherall, P., Wigley, R., 2019. Seafloor Mapping – The Challenge of a Truly Global Ocean Bathymetry. Front. Mar. Sci. 6, 283. https://doi.org/10.3389/fmars.2019.00283.

Wrecksite.eu, 2020. Wrecksite.eu [WWW Document]. URL https://www.wrecksite.eu/ (accessed 1.8.19).